The Time-Dependent Distribution of Phosphorylated Intermediates in Native Sarcoplasmic Reticulum Ca^{2+}-ATPase from Skeletal Muscle Is Not Compatible with a Linear Kinetic Model†

James E. Mahaney,‡ David D. Thomas,§ and Jeffrey P. Froehlich*,||

Department of Biomedical Sciences, Via Virginia College of Osteopathic Medicine, Blacksburg, Virginia 24060, Department of Biochemistry, University of Minnesota Medical School, Minneapolis, Minnesota 55455, and Department of Biochemistry and Molecular Biology, University of Maryland School of Medicine, 108 North Greene Street, Baltimore, Maryland 21201-1503

Received June 20, 2003; Revised Manuscript Received January 21, 2004

ABSTRACT: Quenched-flow mixing was used to characterize the kinetic behavior of the intermediate reactions of the skeletal muscle sarcoplasmic reticulum (SR) Ca-ATPase (SERCA1) at 2 and 21 °C. At 2 °C, phosphorylation of SR Ca-ATPase with 100 μM ATP labeled one-half of the catalytic sites with a biphasic time dependence [Mahaney, J. E., Froehlich, J. P., and Thomas, D. D. (1995) *Biochemistry 34*, 4864−4879]. Chasing the phosphoenzyme (EP) with 1.66 mM ADP 10 ms after the start of phosphorylation revealed mostly ADP-insensitive E2P (95% of EP_{total}), consistent with its rapid formation from ADP-sensitive E1P. The consecutive relationship of the phosphorylated intermediates predicts a decrease in the proportion of E1P ($[E1P]/[EP_{total}]$) with increasing phosphorylation time. Instead, after 10 ms the proportion of E1P increased and that of E2P decreased until they reached a constant 1:1 stoichiometry ($[E1P]:[E2P] \sim 1$). At 21 °C, phosphorylation displayed a transient overshoot associated with an inorganic phosphate (P_i) burst, reflecting increased turnover of E2P at the higher temperature. The P_i burst exceeded the decay of the EP overshoot, suggesting that rephosphorylation of the enzyme occurs before the recycling step (E2 → E1). This behavior and the reversed order of accumulation of phosphorylated intermediates at 2 °C are not compatible with the conventional linear consecutive reaction mechanism: $E1 + ATP \rightarrow E1{\cdot}ATP \rightarrow E1P + ADP \rightarrow E2P \rightarrow E2{\cdot}P_i \rightarrow E1 + P_i$. Solubilization of the Ca-ATPase into monomers using the nonionic detergent $C_{12}E_8$ gave a pattern of phosphorylation in which E1P and E2P behave like consecutive intermediates. Kinetic modeling of the $C_{12}E_8$-solubilized SR Ca-ATPase showed that it behaves according to the conventional Ca-ATPase reaction mechanism, consistent with monomeric catalytic function. We conclude that the nonconforming features of native SERCA1 arise from oligomeric protein conformational interactions that constrain the subunits to a staggered or out-of-phase mode of operation.

The Ca^{2+} pump of sarcoplasmic reticulum (SR)[1] is an adenosinetriphosphatase (SERCA1) that utilizes the energy of ATP hydrolysis to drive uphill Ca^{2+} accumulation. This is accomplished through a specific sequence of protein conformational changes that are linked to the formation and breakdown of chemical intermediates in the Ca-ATPase reaction cycle (see Scheme 1).

Scheme 1

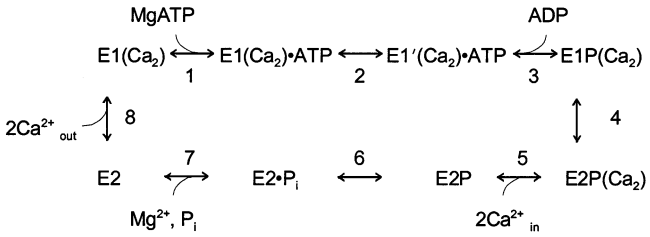

Coupling of the enzymatic reactions to the conformational events enables the chemical energy from ATP to be converted into electrochemical (Ca^{2+} gradient) work. Unidirectional operation of the Ca^{2+} pump relies on an efficient mechanism of energy transduction that involves ATP-driven changes in protein conformation at all levels of structural organization. Ca^{2+} binding at high-affinity sites in the transmembrane domain (*1*) induces changes in the secondary and tertiary structure of the nucleotide (N) and phorphorylation (P) domains that promote high-affinity ATP binding and enzyme phosphorylation (*2*). Likewise, enzyme conformational changes associated with phosphoenzyme formation are transmitted via a long-range intramolecular linkage to

† This work was supported in part by grants to J.E.M. from the American Heart Association, National (EIG 0040094N), and to D.D.T. from the National Institutes of Health (GM27906).

* Corresponding author. Phone: (410) 706-7469. Fax: (410) 706-8297. E-mail: froehlichj@grc.nia.nih.gov.

‡ Via Virginia College of Osteopathic Medicine.

§ University of Minnesota Medical School.

|| University of Maryland School of Medicine.

[1] Abbreviations: SR, sarcoplasmic reticulum; ATP, adenosine 5′-triphosphate; ADP, adenosine 5′-diphosphate; NPE-caged ATP, P^3-[1-(2-nitrophenyl)ethyl]-ATP; EGTA, ethylene glycol bis(aminoethyl ether)-*N*,*N*,*N*′,*N*′-tetraacetic acid; PCA, perchloric acid, TCA, trichloroacetic acid; EPR, electron paramagnetic resonance; IASL, *N*-(1-oxy-2,2,6,6-tetramethyl-4-piperidinyl)iodoacetamide spin label; MOPS, 3-(*N*-morpholino)propanesulfonic acid; $C_{12}E_8$, polyoxyethylene 8 lauryl ether; f_M, mole fraction of the rotationally mobile spectral component; f_R, mole fraction of the rotationally restricted spectral component; EP, acid-stable phosphoenzyme (E1P + E2P); P_i, inorganic phosphate.

10.1021/bi035068g CCC: $27.50
Published on Web 03/19/2004

the high-affinity Ca^{2+} binding sites, changing their orientation toward the SR lumen and lowering their affinity for Ca^{2+} (*3*−*5*). The role of quaternary structure in SERCA1 catalytic function is controversial (*6*−*8*). Indeed, there is evidence to suggest that monomeric Ca-ATPase as depicted in Scheme 1 is fully capable of active Ca^{2+} transport and that protein−protein interactions are not essential for catalytic activity (*6*). Intermolecular interactions have been reported in a number of studies employing kinetic (*9*−*19*) and spectroscopic techniques (*20*−*31*). These contrasting observations raise questions about the specificity of these intermolecular interactions and the role they have in active Ca^{2+} transport.

Studies of the ATP concentration dependence of SERCA1 have shown that, in addition to participating as a substrate for phosphorylation, ATP modulates several of the Ca-ATPase partial reactions after phosphorylation (*7*). Inesi et al. (*32*) and Yamamoto and Tonomura (*33*) found that high (0.2−1 mM) ATP concentrations stimulate overall ATPase activity by an allosteric mechanism involving a low-affinity ATP binding site. Subsequent measurements of the [ATP] dependence of E2P hydrolysis by rapid mixing (*10*) and $P_i \leftrightarrow HOH\ ^{18}O$ exchange (*34*) revealed a separate high-affinity (micromolar range) ATP binding site in the catalytic mechanism. In addition to ATP, the cofactors for phosphorylation, Ca^{2+} and Mg^{2+}, were shown to activate pre-steady-state E2P hydrolysis, suggesting that the high-affinity allosteric site for ATP-dependent regulation involves the neighboring catalytic site in a Ca-ATPase oligomer (*11*). This hypothesis is consistent with X-ray diffraction evidence for a single nucleotide binding site in the crystal structure of SERCA1 (*4*, 5). The vacant site created by the departure of ADP from the catalytic site following E1P formation can accommodate a second molecule of ATP (*8*, *35*) but only weakly binds MgATP (the predominant ATP species in the assay) because of steric hindrance by Mg^{2+} bound at the catalytic site. This suggests that the phosphorylated enzyme does not contain the high-affinity allosteric site for the activation of E2P hydrolysis by MgATP (*10*, *34*).

Rapid mixing studies of phosphorylation by ATP (*36*) suggest that the kinetics of this reaction is controlled by a conformational change that is induced by MgATP binding and that leads to the formation of a second Michaelis complex, $E1'(Ca_2)\cdot MgATP$ (step 2, Scheme 1). This transition has been studied by fluorescence spectroscopy (*22*, *37*−*40*) and by electron paramagnetic resonance (EPR) spectroscopy (*41*−*43*) using an iodoacetamide spin label (IASL) covalently attached to Cys-674 in the cytoplasmic domain of the transport protein (*44*). The interaction of various ligands (ATP, ADP, AMPPCP) with the catalytic site induces a conformational change that restricts the rotational mobility of a specific fraction of these EPR spin probes, producing a resolved EPR signal component corresponding to strong immobilization. This signal coincides with the appearance of $E1'(Ca_2)\cdot MgATP$ and persists during the formation of $E1P(Ca_2)$ (*45*−*47*) but is not produced by back-door phosphorylation of the enzyme using P_i (*48*). On the basis of these results, the immobilized EPR signal is believed to monitor the formation of ADP-sensitive E1P (which is rate-limited by $E1'(Ca_2)\cdot MgATP$ formation) and disappear upon its conversion to ADP-insensitive E2P. The persistence of this EPR signal under steady-state cycling conditions is consistent with the results of ADP chase experiments demonstrating the presence of high levels of E1P during ATP-dependent phosphorylation (*9*).

We previously reported (*12*) the kinetic characterization of the IASL EPR signal associated with the first turnover of the Ca^{2+} pump in SR membrane vesicles at 2 °C. Synchronous activation of Ca-ATPase was achieved by laser flash photolysis of NPE-caged ATP, a protected ATP analogue (reviewed in ref *49*). An unusual feature of the EPR signal was its correlation with a slow, secondary phase of acid-stable phosphoenzyme formation produced by mixing the Ca^{2+}-liganded enzyme with MgATP. The biphasic phosphorylation pattern at 2 °C, which is accentuated by high [KCl], was resolved into fast and slow phases, suggesting parallel reaction pathways. Raising the [KCl] from 0.1 to 0.4 M resulted in concomitant slowing of the secondary phase of phosphorylation and the transient EPR signal without affecting the kinetics of the fast phosphorylation reaction. We attributed the kinetic heterogeneity of phosphoenzyme formation to a Ca-ATPase dimer in which the protomers are coupled through a conformational interaction, permitting only staggered or out-of-phase operation during cycling (*12*):

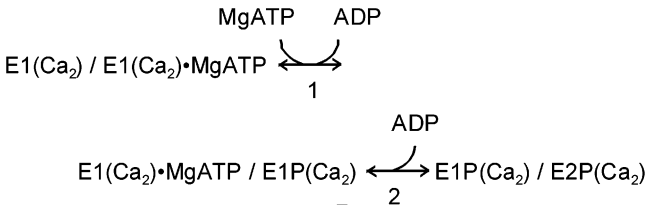

Conformational coupling delays the left-hand subunit relative to its partner in carrying out the catalytic transformations of the Ca^{2+} pump (*13*), resulting in the stable asymmetrical oligomeric intermediate, $E1P(Ca_2)/E2P(Ca_2)$ (step 2). The presence of this species accounts for the similar proportions of E1P and E2P in the steady state (*12*) and the rapid pre-steady-state accumulation of both phosphorylated intermediates in the absence of a highly reversible E1P ↔ E2P transition (*9*). Elimination of oligomeric coupling destabilizes E1P, thus accounting for its disappearance following solubilization of SERCA1 with the monomer-forming detergent $C_{12}E_8$ (*14*, *52*). To explain the absence of a rapid EPR signal corresponding to the formation of $E1(Ca_2)\cdot MgATP/E1P(Ca_2)$ in the first step, one can assume that the second step is very fast, which would rapidly deplete signal-producing E1P on the right-hand subunit. This is consistent with quenched-flow evidence demonstrating rapid accumulation of E2P at 21 °C (*9*), but conflicts with observations at 2 °C (*12*) in which the secondary phase of phosphorylation and the corresponding EPR signal controlled by step 2 obey slow kinetics. It is not known how rapidly E1P is converted to E2P in the pre steady state at 2 °C or whether the slow EPR signal monitors some other conformational change in the transport protein controlling phosphorylation. Additional experiments are needed to determine the origin of the EPR signal and the kinetics of the E1P → E2P transition at reduced temperatures.

In the present study, we monitored the kinetics of E1P and E2P formation at 2 °C in two-stage quenched-flow mixing experiments using ADP or ADP + high [Ca^{2+}] to chase the phosphoenzyme formed from MgATP. Several laboratories have reported that dephosphorylation by ADP

produces fast and slow phases of phosphoenzyme decay (*53*−*56*). Froehlich and Heller (*9*) showed that inorganic phosphate (P_i) production accompanies the slow decay phase at 21 °C and that mixing with ADP + millimolar Ca^{2+} ([Ca^{2+}]-jump conditions) accelerates dephosphorylation and concomitant P_i production while decreasing total P_i production. These features are consistent with a model in which the initial decay represents the disappearance of E1P to E1·ATP (reversal of phosphorylation), while the slow decay corresponds to the transformation of E2P to E2 and P_i (at low [Ca^{2+}]) or to E1·ATP via E1P (at high [Ca^{2+}]). In this study, the relative proportions of the acid-stable intermediates were monitored over time using a phosphoenzyme chase solution containing 5 mM ADP alone or with 15 mM Ca^{2+} added to distinguish the presence of E2P. A parallel set of quenched-flow experiments was carried out using the $C_{12}E_8$-solubilized (monomeric) Ca-ATPase for comparison with the native membranous enzyme. The results of the ADP chase experiments in the native enzyme at 2 °C conflict with the predictions of the Albers−Post model or any purely linear reaction scheme in which E1P and E2P are consecutive intermediates. A revised mechanism that accommodates our results assumes that the native Ca-ATPase is an oligomer with coupled parallel catalytic pathways that operate out of phase with each other. In contrast to native SERCA1, the $C_{12}E_8$-solubilized enzyme demonstrated kinetic behavior that was fully consistent with monomeric catalysis as shown in Scheme 1. We conclude that steady-state E1P accumulation in SERCA1 is associated with Ca-ATPase oligomer formation and that the intermolecular conformational interactions reflected in this behavior play an important role in vectorial Ca^{2+} transport catalyzed by the fast skeletal muscle Ca-ATPase isoform.

MATERIALS AND METHODS

Reagents and Solutions. Polyoxyethylene 8 lauryl ether, or $C_{12}E_8$ (Nikko Chemicals, Tokyo), was twice recrystallized from diethyl ether to remove impurities. The white crystalline material was stored under dry nitrogen at −20 °C. The calcium ionophore A23187 was obtained from Calbiochem, and ATP and MOPS were obtained from Sigma. All other reagents were of the highest purity available. Unless otherwise noted, all quenched-flow experiments were carried out in a buffer containing 5 mM $MgCl_2$, 0.45 mM $CaCl_2$, 0.5 mM EGTA (3.5 μM free Ca^{2+}), 20 mM MOPS, pH 7.0 (henceforth denoted standard buffer), and a [KCl] of either 0.1 or 0.4 M, as indicated.

Preparations and Assays. Sarcoplasmic reticulum (SR) vesicles were prepared from the fast twitch skeletal muscle of New Zealand white rabbits as described previously (*12*). SR vesicles prepared in this fashion were typically 75% Ca-ATPase (∼7 nmol of Ca-ATPase/mg of SR) and contained approximately 80 mol of phospholipid/mol of Ca-ATPase (*57*). Calcium-dependent ATPase activity of Ca^{2+} ionophore (A23187) treated SR vesicles was measured as described in Squier and Thomas (*58*). SR protein concentrations were determined by the biuret assay (*59*) using bovine serum albumin as a standard. For preparation of monomeric Ca-ATPase, the native enzyme was solubilized by exposure to the nonionic detergent, $C_{12}E_8$ (*50*), at a 10:1 ratio of detergent to SR protein in the following medium: 0.1 M KCl, 3 mM $MgCl_2$, 1.5 mM $CaCl_2$, 1 mM EGTA, 50 μM mercaptoethanol, and 20 mM TES buffer, pH 7.0 at 21 °C (*52*). The insoluble residue was separated from the solubilized enzyme by centrifugation at 140000*g* for 1 h at 4 °C and the protein concentration determined by the Petersen modification of the Lowry procedure (*60*).

ATP-Dependent Phosphoenzyme Formation. Rapid mixing studies were performed as described by Froehlich and Heller (*9*) using a quenched-flow apparatus equipped for one- and two-stage mixing operations (*61*). Measurements were carried out at room temperature (21 ± 0.5 °C) or at 2 ± 0.5 °C by conducting the experiments in a cold room. The enzyme- and substrate-containing syringes both contained 5 mM $MgCl_2$, 0.45 mM $CaCl_2$, 0.5 mM EGTA, 20 mM MOPS, pH 7.0, and 0.1 M KCl. The enzyme syringe also included the calcium ionophore, A23187 (1 μg/0.05 mg of SR protein), to prevent intravesicular Ca^{2+} accumulation. Phosphoenzyme formation was initiated by mixing SR vesicles (0.5 mg/mL) with an equal volume of the substrate medium containing 20 or 200 μM [γ-^{32}P]ATP. After a variable time delay (4−300 ms), the reaction was terminated by the addition of 3% perchloric acid + 2 mM H_3PO_4 (final concentrations). The assays for the [^{32}P]phosphoenzyme and [^{32}P]P_i in the acid-quenched reaction mixture were carried as previously described (*9*, *12*). Protein recovery following the washing procedure was greater than 95% as determined by protein assay. Radioisotope in the protein pellet and in the charcoal-extracted supernatant was determined by counting the Cerenkov radiation of samples mixed with 1 N NaOH.

Dephosphorylation of the Phosphoenzyme by ADP. ADP dephosphorylation experiments at 2 and 21 °C were carried out as described previously by Froehlich and Heller (*9*). SR vesicles (0.375 mg/mL) were made permeable to Ca^{2+} with A23187 (1 μg/0.05 mg of SR protein) except in the experiments with passively loaded vesicles (see below). The membranes were phosphorylated as described above with 20 μM or 0.2 mM [γ-^{32}P]ATP for a pre-set time interval, *t* (6, 10, 116, and 223 ms). Dephosphorylation by ADP was initiated by mixing 2 volumes of the phosphorylation reaction mixture with 1 volume of a chase solution containing 5 mM ADP (1.66 mM final concentration), 100 mM KCl, 5 mM $MgCl_2$, 0.45 mM $CaCl_2$, 0.5 mM EGTA, and 20 mM MOPS, pH 7.0. After a variable time delay (0−300 ms), the dephosphorylation reaction was terminated with 3% perchloric acid + 6 mM H_3PO_4 and the quenched reaction mixture assayed for ^{32}P-labeled phosphoenzyme and [^{32}P]P_i as described previously (*9*, *12*). In the [Ca^{2+}]-jump experiments, EGTA was left out of the dephosphorylation chase which contained 15 mM $CaCl_2$ in addition to 5 mM ADP to give a final Ca^{2+} concentration of 5 mM after mixing. For ADP dephosphorylation experiments using Ca^{2+}-preloaded SR vesicles, native SR vesicles (0.75 mg/mL) were passively loaded with 5 mM $CaCl_2$ for 6 h on ice in a medium containing 50 mM KCl, 5 mM $CaCl_2$, 3 mM $MgCl_2$, and 40 mM MOPS, pH 6.8. To initiate phosphoenzyme formation, Ca^{2+}-loaded vesicles at 21 °C were mixed with an identical solution containing 20 μM [γ-^{32}P]ATP and 5 mM EGTA without added $CaCl_2$. Chelation of the Ca^{2+} by EGTA after mixing rapidly lowered the extravesicular free [Ca^{2+}] to ∼100 μM. The higher buffer concentration employed in these experiments (40 mM MOPS) was used to prevent an acid shift in the pH from the protons released from EGTA upon

chelation of Ca^{2+}. Dephosphorylation was initiated by mixing with a solution containing 5 mM ADP with or without 15 mM $CaCl_2$ as described above. Control, unloaded SR vesicles were treated in a similar fashion, except that $CaCl_2$ was omitted from the buffer during the 6 h incubation on ice, and the membrane vesicles were phosphorylated with a solution containing 20 μM [γ-^{32}P]ATP and 0.1 mM $CaCl_2$.

Quenched-Flow Experiments with $C_{12}E_8$-Solubilized Ca-ATPase. The nonionic detergent, $C_{12}E_8$ (polyoxyethylene 8 lauryl ether), solubilizes the SR Ca-ATPase into monomers with retention of enzymatic activity (*50*). Active Ca-ATPase monomers were prepared using $C_{12}E_8$ (Nikko Chemicals) and the conditions for solubilization described by Andersen et al. (*52*). The solubilized enzyme (0.5 mg/mL) was suspended in a medium containing 100 mM KCl, 3 mM $MgCl_2$, 1.5 mM $CaCl_2$, 1 mM EGTA, 50 μM mercaptoethanol, and $C_{12}E_8$ (5 mg/mL) and mixed at 21 °C with an equal volume of the substrate medium of identical ionic composition containing 20 μM [γ-^{32}P]ATP. Samples obtained at the beginning and the end of the rapid mixing experiment showed similar phosphorylation activity. Determination of the phosphorylated protein in the acid-quenched samples was the same as in the native enzyme except that 200 μL of 1% deoxycholic acid was added to each sample tube to quantitatively precipitate the ^{32}P-labeled phosphoprotein. In the inorganic phosphate assay, the presence of detergent necessitated two extractions with activated charcoal to remove the unhydrolyzed nucleotide prior to forming the phosphate−molybdate complex. Dephosphorylation was accomplished by chasing the phosphoenzyme with a solution containing 5 mM ADP (1.66 mM, final), 100 mM KCl, 3 mM $MgCl_2$, and 20 mM TES, pH 7.0 at 21 °C. The ADP chase was added after 6 and 116 ms of phosphorylation to monitor the accumulation of the phosphorylated intermediates (E1P and E2P) during the pre-steady state and steady state of phosphorylation, respectively. In a few experiments, 5 mM $CaCl_2$ was included in the ADP chase solution ([Ca^{2+}]-jump conditions) to induce Ca^{2+} binding to the low-affinity sites on E2P and stimulate its breakdown in the direction of E1·ATP (*9*).

Curve Fitting and Kinetic Modeling. Dephosphorylation induced by chasing with ADP exhibited a fast phase (not resolved) corresponding to the disappearance of E1P, a secondary phase corresponding to the disappearance of E2P, and a very slow phase, representing the decay of a stable phosphoenzyme component, ESP (*9*). ADP-induced phosphoenzyme decomposition was modeled with a multiexponential function using the Marquardt−Levenberg-based routines contained in MLAB (*62*). The best fit was achieved with a triexponential decay function:

$$[EP]_t = A_1 \exp(-k_1 t) + A_2 \exp(-k_2 t) + A_3 \exp(-k_3 t) \quad (1)$$

where A_i and k_i are the amplitude coefficient and rate constant, respectively, for the ith decay phase ($i = 1, 2, 3$). For each experiment, the best fit was chosen on the basis of optimization of the determination coefficient, R^2, and minimization of the difference between the fitted curve and data points (sum-of-squares error). Initial values for the amplitude (A_i) and rate (k_i) parameters were obtained from semilog plots of the data; these were allowed to vary without bound during the fit constrained only to the range of positive numbers ($A_i = 0$; $k_i = 0$). Iteration was continued until the fit converged (indicated by unchanging R^2 and sum-of-squares error between successive iterations).

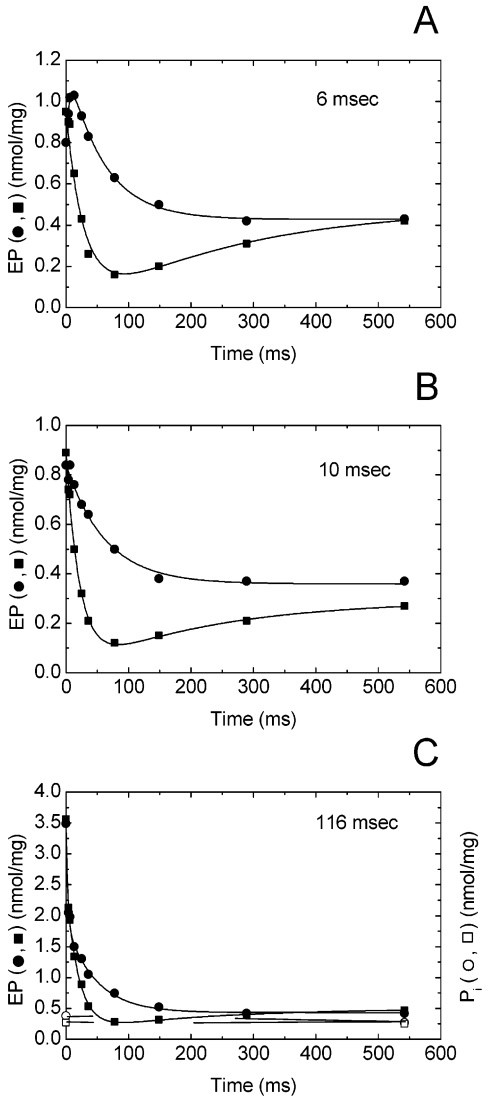

FIGURE 1: Phosphoenzyme decomposition in the presence of 0.1 M KCl at 2 °C following the addition of ADP or ADP + Ca^{2+} ([Ca^{2+}] jump) to SR vesicles phosphorylated for 6 ms (panel A), 10 ms (panel B), or 116 ms (panel C). SR vesicles (0.375 mg of protein/mL), permeabilized with the Ca^{2+} ionophore A23187 (1 μg/0.05 mg of SR protein), were phosphorylated by 0.1 mM [γ-^{32}P]-ATP in a solution containing 100 mM KCl, 5 mM $MgCl_2$, 0.45 mM $CaCl_2$, 0.5 mM EGTA (3.5 μM ionized Ca^{2+}), and 20 mM MOPS (pH 7.0). After 6, 10, or 116 ms of phosphoenzyme formation, either (filled circles) 1.66 mM ADP or (filled squares) 1.66 mM ADP + 5 mM $CaCl_2$ (final concentrations) was added, and the reaction was terminated at the indicated times by the addition of 3% perchloric acid + 2 mM H_3PO_4. In the dephosphorylation experiment using SR vesicles phosphorylated for 116 ms (panel C), inorganic phosphate (P_i) liberation following the addition of (open circles) 1.66 mM ADP or (open squares) 1.66 mM ADP + 5 mM $CaCl_2$ (final concentrations) was also measured. The curves through the data points represent the best fits using the parameters listed in Table 1.

We experienced two complications in applying eq 1 to the ADP chase data. First, ADP-induced phosphoenzyme decay did not always conform to a simple pattern, but in some cases EP increased briefly prior to decaying (cf. Figure 1A, filled circles) or increased slowly after an initial decay (cf. Figure 1A−C, filled squares). The former situation reflects continued phosphorylation from bound ATP (E1·

ATP) after addition of the ADP chase while the latter reflects "rebound" phosphorylation after chasing with ADP + high [Ca^{2+}] ([Ca^{2+}] jump). In both cases, we fit the data using the equation:

$$[EP]_t = A_1 \exp(-k_1 t) + A_2 \exp(-k_2 t) + A_3 \qquad (2)$$

where A_3, representing the level of the residual or stable phosphoenzyme, is equal to the sum of A_1 and A_2. In the former case, k_1 and k_2 correspond respectively to the brief rise and slow ADP-induced decay following the decay, while in the latter case they correspond to the rapidly decaying and slowly rising (rebounding) phases of phosphorylation. In experiments where an initial fast decay appeared prior to the slow decay and/or rebound behavior (Figure 1B,C, filled circles and squares), the data were fit with eq 2 using the 4 ms data point as a zero-time point. This reduced the number of exponentials in the fit from 3 to 2, but did not affect the kinetic parameters because EP decomposition prior to 4 ms is not time-resolved (see below).

The second problem in modeling the ADP chase data involved the initial decay, which corresponds to the resynthesis of ATP by reversal of step 3: ADP + E1P(Ca_2) ↔ E1′(Ca_2)·ATP. Attempts to fit this phase to an exponential decay led to an underestimation of its rate and overestimation of its amplitude because the curve-fitting program assumes that the first resolved data point (usually at $t = 4$ ms) after addition of the ADP chase (at zero time) lies on the fast phase. We have evidence that the fast decay does not reflect the enzymatic reversal of phosphorylation but, instead, represents a chemical transformation in the acid-denatured protein after the quench has been added (see Results and Discussion). To circumvent this problem, we assigned the initial phase an arbitrarily large rate ($k_1 > 1000$ s^{-1}) so that its decay is complete prior to the 4 ms data point. In this approximation, phosphoenzyme measured at 4 ms consists only of E2P plus the stable phosphoenzyme, ESP. Values for the decay rate constants (k_2, k_3) and amplitude coefficients ($[E2P]_0$, $[ESP]_0$) for E2P and ESP were obtained from the computer-generated fit to the curve defined by the data points between 4 and 542 ms. Since the zero-time phosphoenzyme, $[EP_{total}]_0$, consists of three species, [E1P], [E2P], and [ESP], the amount of E1P at zero time can be calculated by subtraction of the other two components:

$$[E1P]_0 = [EP_{total}]_0 - [E2P]_0 - [ESP]_0 \qquad (3)$$

The fraction of phosphoenzyme present as E1P at $t = 0$ equals $100[E1P]_0/([E1P]_0 + [E2P]_0)$, where the contribution from the stable component, ESP, is not included in the calculation because it arises parallel to the main catalytic pathway (*9*). An analogous expression was used to calculate the fraction of phosphoenzyme present as E2P.

The kinetic model used for simulating time-dependent EP and P_i formation measured in the single-stage quenched-flow experiments at 21 °C is a simplified version of the Albers−Post scheme shown in Scheme 1:

$$E1 + ATP \underset{1}{\leftrightarrow} E1{\cdot}ATP \underset{2}{\leftrightarrow} E1P + ADP \underset{3}{\leftrightarrow} E2P \underset{4}{\leftrightarrow} E2{\cdot}P_i \underset{5}{\leftrightarrow} E1 + P_i \qquad (4)$$

The distribution of intermediates in the reaction cycle is determined by the forward, k_i, and reverse, k_{-i}, rate constants, where $i = 1, 2, 3, 4, 5$. The formation and breakdown of the reaction cycle intermediates over time are each defined by a differential equation of the form (*63*):

$$d[A_j]/dt = \sum k_m[A_k] - \sum k_n[A_j] \qquad (5)$$

where A_j and A_k ($j \neq k$) are intermediates, k_m and k_n are rate constants, the first term on the right represents the sum of reactions producing A_j, and the second term represents the sum of reactions converting A_j to precursors and products. The kinetic model in eq 4 is defined by a set of seven differential equations and a conservation equation relating the total enzyme concentration, $[E_{total}]$, to the sum of the intermediate concentrations (see Appendix). Computer simulations of EP (E1P + E2P) formation and P_i release were done by simultaneously integrating the set of equations derived from the model using MLAB (*62*). Initially ($t = 0$), $[E_{total}] = [E1]$, and all other intermediates and products have a value of zero. The back-reactions for ADP and P_i release were neglected because product formation during the initial stages of ATP hydrolysis is negligible. All of the reactions with the exception of step 1, involving ATP binding to E1, and step 4, involving the reversible hydrolysis of E2P (*34*), were modeled as irreversible reactions. Initial values for the rate constants, k_i and k_{-i}, were obtained from the literature (*9*−*11*). Visual inspection was used with trial-and-error adjustment of the kinetic parameters to optimize the computer-generated fit of the model to the experimental data.

RESULTS

Dephosphorylation of the Phosphoenzyme by ADP at 2 °C in the Presence of 0.1 M KCl. Results obtained in an earlier study (*12*) comparing pre-steady-state phosphoenzyme formation and accumulation of the strongly immobilized fraction of IASL in Ca-ATPase at 2 °C suggested that the conversion of E1P to E2P during the initial turnover is very fast. To determine how rapidly the conversion of E1P to E2P takes place after phosphorylation under these conditions, we measured the fraction of ADP-sensitive phosphoenzyme, E1P, formed at various times after mixing with ATP. The presence of E1P was evaluated from the initial rapid phase of dephosphorylation produced by chasing the phosphoenzyme with ADP (*9*, *12*). These experiments were performed at 0.1 M KCl where phosphoenzyme accumulating in the fast (49 s^{-1}) and slow (20 s^{-1}) phases was present at a ratio of 5:1.

Figure 1 shows the pattern of phosphoenzyme decomposition induced by the addition of 1.33 mM ADP after 6 (panel A), 10 (panel B), and 116 ms (panel C) of phosphorylation with 100 μM ATP. These times were selected to characterize the relative proportions of E1P and E2P during the pre-steady state (panels A and B) and steady state of phosphorylation (panel C). The dephosphorylation pattern in each experiment was triphasic, consisting of an unresolved rapidly decaying component, an intermediate (25 s^{-1}) component, and a very slowly decaying (~1 s^{-1}) residual phosphoenzyme. Inorganic phosphate (P_i) production measured in the 116 ms ADP chase experiment (Figure 1C) was <0.2 nmol of P_i/mg of protein at zero time (equal to ~6% of the corresponding EP level) and remained essentially unchanged out to 300 ms where the phosphoenzyme had almost completely disappeared. The

unchanging P_i level in Figure 1C indicates that the enzyme-bound phosphate in both acid-stable intermediates is fully reconverted to ATP under these conditions. This contrasts sharply with the behavior seen at 21 °C where the higher temperature increased the zero-time P_i production to 50% of the corresponding EP level and where the intermediate component of ADP-induced dephosphorylation (E2P) decayed stoichiometrically to P_i (cf. Figures 4 and 5). By analogy to the ADP dephosphorylation pattern at 21 °C, the rapid decay phase measured at 2 °C corresponds to the resynthesis of E1·ATP from E1P while the intermediate phase results from the decomposition of E2P to E1·ATP. The residual phosphoenzyme that follows the intermediate phase turns over too slowly to be in the main catalytic pathway (*9*).

Attempts to resolve a time point on the fast decay phase have repeatedly failed, even after lowering the ADP concentration (*9*) and reducing the reaction time to <3 ms with back-to-back ball mixers. An analysis of the rate constants involved in dephosphorylation of the ADP-sensitive phosphoenzyme indicated that the fast decay does not represent the normal enzymatic activity associated with the reversal of phosphorylation (see Discussion). Instead, it might result from the acid-catalyzed transmigration of enzyme-bound phosphate from E1P·ADP to ATP immediately following the acid quench. In that case, the amplitude of the fast decay is equal to [E1P] present when the ADP chase is added because the E1P is fully complexed with ADP prior to acid quenching. Because data points on the fast decay phase could not be time-resolved, computer fitting of these data to a sum of exponentials resulted in an underestimation of the rate constant for dephosphorylation of E1P and an overestimation of its amplitude. Consequently, an alternative procedure (see Materials and Methods) was used to evaluate the amplitudes of the fast and intermediate decay components based on the assumption that E1P·ADP disappears completely from the EP pool after the quench has been added. What remains are only the ADP-insensitive (E2P) and stable phosphoenzymes, which are acid-stable in the presence of ADP and exhibit decay patterns that reflect their prequench turnover kinetics.

An unexpected finding was that the phosphoenzyme accumulating at very early times (6 and 10 ms, panels A and B of Figure 1, respectively) consists mainly of ADP-insensitive E2P (Table 1). According to Scheme 1, the predominant phosphorylated species in the early pre-steady state is E1P, which should disappear over time as E2P builds up. The phosphoenzyme formed after 6 ms of phosphorylation continued to rise briefly following ADP addition (Figure 1A), indicating that γ-phosphoryl transfer from bound ATP to the enzyme continues after the ADP has been added. There was no evidence of a fast decay component in the dephosphorylation time course following the initial rise in the EP level. After 10 ms of phosphorylation (Figure 1B), E1P accounted for only ~3% of the total EP, suggesting that E1P is almost fully converted to E2P during the first 10 ms after mixing with ATP. When the ADP chase was added after 116 ms, which corresponds to the steady state of phosphorylation (*12*), the amount of E1P had increased to 47% of the total EP (Figure 1C). Thus, between 10 and 116 ms the fraction of E1P *rose* from a few percent to about one-half of the total EP. These results are incompatible with the reaction sequence in Scheme 1, which predicts that the proportion of the ADP-sensitive phosphoenzyme, [E1P]/[EP_{total}], should decrease with time as the proportion of the ADP-insensitive phosphoenzyme, [E2P]/[EP_{total}], increases.

Table 1: ADP-Induced and ADP + Ca^{2+}-Induced Dephosphorylation of SR Ca-ATPase at 0.1 M KCl and 2 °C[a]

dephosphorylation conditions	phosphorylation time (ms)	[E1P] (nmol/mg)	k_1 (s^{-1})	[E2P] (nmol/mg)	k_2 (s^{-1})	% E1P
1.66 mM ADP	6	nd	−	0.37	11	0
1.66 mM ADP + 5 mM $CaCl_2$	6	nd	−	0.52	21	0
1.66 mM ADP	10	0.02	nr	0.78	10	2.5
1.66 mM ADP + 5 mM $CaCl_2$	10	0.04	nr	0.82	24	4.7
1.66 mM ADP	116	1.44	nr	1.63	25	47
1.66 mM ADP + 5 mM $CaCl_2$	116	1.39	nr	1.63	43	46

[a] ADP-induced dephosphorylation in Figure 1 was fit using the triexponential decay function $[EP]_t = A_1 \exp(-k_1 t) + A_2 \exp(-k_2 t) + A_3 \exp(-k_3 t)$, where A_1 and A_2 and k_1 and k_2 are the amplitude coefficients and decay rate constants of the ADP-sensitive (E1P) and ADP-insensitive (E2P) phosphoenzymes, respectively, and A_3 and k_3 correspond to a residual phosphoenzyme species (*9*). Initial values for A_i and k_i were obtained from semilog plots of the EP decay data but were allowed to vary freely during the fit. For dephosphorylation following either 10 or 116 ms of phosphorylation, the fast component (k_1) was present but not resolved (nr) (see Results). A fast decay component was not detected (nd) after 6 ms of phosphorylation. Rate constants for the dephosphorylation experiments at 6 ms were evaluated using eq 2 as described in Materials and Methods.

Additional dephosphorylation experiments were carried out at 2 °C in 100 mM KCl using 1.66 mM ADP + 5 mM Ca^{2+} ([Ca^{2+}]-jump conditions) to confirm the presence of E2P in the intermediate decay phase. At 21 °C, jumping the [Ca^{2+}] causes E2P to disappear more rapidly during the ADP chase by reversal of steps 5 (Ca^{2+} binding to E2P), 4 (conversion of E2P(Ca_2) to E1P(Ca_2)), and 3 (formation of E1P(Ca_2)·ATP from E1′P(Ca_2)·ADP in Scheme 1 (*9*). To allow Ca^{2+} access to the low-affinity (luminal) transport sites on E2P, the SR vesicles were pretreated with the Ca^{2+} ionophore A23187 (see Discussion). As shown in Figure 1C (square symbols), dephosphorylation by ADP + Ca^{2+} produced a triphasic decay pattern in which the intermediate component disappeared more rapidly (2-fold; Table 1) than with ADP added alone. After an initial decline, the intermediate decay component rose again slowly (~11 s^{-1}). This rebound phenomenon may have resulted from transient dephosphorylation of the stable component and its recovery to the steady-state level measured in the absence of the [Ca^{2+}] jump. The accelerated decay of the intermediate component at high [Ca^{2+}] is characteristic of the ADP-insensitive phosphoenzyme, E2P, which contains low-affinity binding sites for Ca^{2+} (*9*, *54*) that are occupied during the [Ca^{2+}] jump. This is necessary for the reversal of step 4 and the formation of E1P(Ca_2), which rapidly combines with ADP to form E1·ATP. No inorganic phosphate (P_i) production was observed after chasing with ADP (Figure 1C, open circles) or under [Ca^{2+}]-jump conditions (Figure 1C, open squares). The absence of P_i release during the intermediate decay phase at 2 °C implies that Ca^{2+} remains associated with E2P after the E1P → E2P transition (possibly in an occluded form) and is, therefore, able to activate reversal of this reaction following the addition of ADP. Evidently, the low-affinity transport sites in the Ca^{2+}-occluded state are

incompletely saturated or release Ca^{2+} during the ADP chase because jumping the [Ca^{2+}] from ~10 μM to 5 mM accelerated E2P decay compared to nonjump conditions.

Chasing the phosphoenzyme formed during the pre-steady state of phosphorylation with 1.66 mM ADP + 5 mM $CaCl_2$ increased the rate of dephosphorylation of the intermediate component (Figure 1A−C, filled squares) compared to chasing with ADP alone (closed circles). The accelerated phosphoenzyme decay induced by the [Ca^{2+}] jump implies that the intermediate decay component observed 6−10 ms after mixing with ATP is ADP-insensitive E2P. The possibility that it represents an ADP-sensitive species (*56*) is excluded on the grounds that the Ca^{2+} transport sites activating E1P formation have an affinity in the micromolar range (*64*) and do not increase their level of occupation during the [Ca^{2+}] jump. Taken together, these results imply that the isomerization of E1P to E2P occurs very rapidly during the first turnover despite the reduced (2 °C) temperature. The rapid accumulation of E2P during the initial stages of phosphorylation is followed paradoxically by an increase in the fraction of E1P, which rose to the same level as E2P. Following the transition Ca^{2+} associated with E2P remains occluded, consistent with the absence of a pre-steady-state burst of internal Ca^{2+} release in arsenazo III-loaded SR vesicles at 2 °C (*65*). At 21 °C, the presence of occluded Ca^{2+} in the ADP-insensitive phosphoenzyme [E2P(Ca_2) in Scheme 1] was used to explain the delay in pre-steady-state $^{45}Ca^{2+}$ sequestration following the rapid accumulation of E2P (*9*).

ATP-Dependent Phosphoenzyme Formation at 21 °C. Maximum steady-state phosphorylation levels measured in native SERCA1 are similar at 2 and 21 °C (~3.5 nmol/mg at 100 μM ATP), but P_i production differs markedly. At 21 °C, increased turnover of the phosphoenzyme leads to an initial burst of P_i production (*10*) that is completely absent at the lower temperature (Figure 1C). The P_i burst is associated with a transient decrease in the phosphoenzyme level, resulting in an overshoot. The decay of the overshoot and P_i burst were both accelerated by raising the ATP concentration (*10*). These observations are compatible with a model in which E2P hydrolysis produces a noncovalent intermediate, E2·P_i, that turns over slowly releasing P_i. Analog computer simulations of EP and P_i formation using a simple four-state model were shown to reproduce the general features of the data with the assumption that the kinetics of E2·P_i formation and breakdown vary with the ATP concentration (*10*). Attempts to achieve a quantitative fit to the behavior of these reactions were unsuccessful, particularly at ATP concentrations >5 μM where the steady-state EP level does not decay due to substrate depletion (unpublished observations).

To confirm our previous findings and to test the model by simulation, we conducted single-stage quenched-flow experiments at 21 °C measuring ATP-dependent phosphorylation and P_i release in the presence of 10 μM (Figure 2A) and 100 μM ATP (Figure 2B) using a standard buffer containing 0.1 M KCl. In each case, the EP level increased rapidly to a maximum, followed by a slower decline to a steady-state level. The apparent rate of phosphorylation increased roughly 2-fold between 10 and 100 μM ATP, while the steady-state EP level rose by 14% (3.2−3.7 nmol of EP/mg of SR protein), reflecting increasing saturation of the catalytic site by ATP. Phosphate liberation exhibited a brief lag during the initial formation of phosphoenzyme, followed by a burst phase and a linear steady state as reported previously (*9*−*11*). Extrapolation of the linear phase of P_i production to $t = 0$ gave P_i burst amplitudes of 1.0 and 1.5 nmol of P_i/mg of protein at 10 and 100 μM ATP, equaling 30−40% of the EP levels measured. This is less than half the value reported originally (*10*) but is similar to the amplitudes found in subsequent measurements by us (*9*). Extrapolation of linear P_i production to the *y*-axis underestimates the steady-state level of catalytic intermediate(s) in the burst phase because it ignores the initial lag in P_i production preceding the linear (steady-state) phase of ATP hydrolysis. When P_i production was simulated using the model in eq 4 (see Materials and Methods), the concentration of dephosphorylated enzyme (present as E2·P_i and/or E2) in the burst phase increased to almost half (48%) of the steady-state EP level at 100 μM ATP. Using simulation, the sum of the phosphorylated and dephosphorylated intermedi-

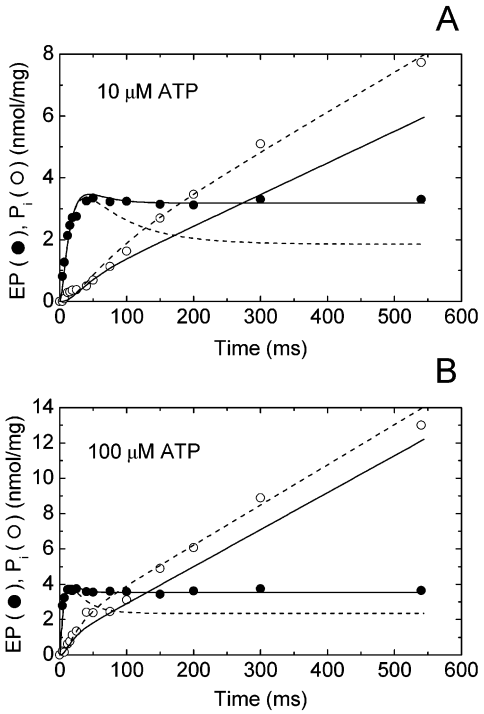

FIGURE 2: Phosphoenzyme (EP) formation and phosphate (P_i) release at 21 °C in the presence of 0.1 M KCl and either 10 μM (panel A) or 100 μM [γ-^{32}P]ATP (panel B). SR vesicles (0.25 mg/mL) were phosphorylated in a solution containing 100 mM KCl, 5 mM $MgCl_2$, 0.45 mM $CaCl_2$, 0.5 mM EGTA (3.5 μM ionized Ca^{2+}), and 20 mM MOPS (pH 7.0). At the indicated times the reaction was terminated by the addition of 3% perchloric acid + 2 mM H_3PO_4. Phosphoenzyme formation (filled circles) and P_i release (open circles) were measured as described in Materials and Methods. The time course of EP formation and P_i release was simulated using the rate constants and kinetic scheme shown in Table 2. Solid lines were generated using either $k_4/k_{-4} = 7\ s^{-1}/14\ s^{-1}$ and $k_5/k_{-5} = 12\ s^{-1}/0$ (panel A, 10 μM ATP) or $k_4/k_{-4} = 20\ s^{-1}/40\ s^{-1}$ and $k_5/k_{-5} = 20\ s^{-1}/0$ (panel B, 100 μM ATP). These parameters gave the best fit to the time course of phosphoenzyme formation but underestimated the burst phase of P_i release. Dashed lines were generated using either $k_4/k_{-4} = 7\ s^{-1}/0$ and $k_5/k_{-5} = 6\ s^{-1}/0$ (panel A, 10 μM ATP) or $k_4/k_{-4} = 20\ s^{-1}/9.5\ s^{-1}$ and $k_5/k_{-5} = 9.5\ s^{-1}/0$ (panel B, 100 μM ATP). These parameters reproduced the time course of P_i liberation but underestimated steady-state phosphoenzyme formation. Additional details of the simulations are given in the text.

ates is 5.5 nmol/mg of protein, which is 20−25% lower than the density of enzymatic sites found in the SR membrane (~7 nmol/mg of protein). This suggests that an additional unphosphorylated species (E1·ATP?) is present at significant levels during steady-state enzymatic cycling.

We previously reported (*10*) that subsaturating ATP concentrations (low micromolar range) stimulate dephosphorylation as well as the linear phase of ATP hydrolysis following the burst, reflecting modulation of the rate-limiting conformational transition, E2 → E1. The kinetic data of Figure 2 were simulated (solid and dashed lines) using a simplified version of the Albers−Post model in Scheme 1 (see Materials and Methods) and by integrating the differential equations for this model using MLAB (see Appendix). The kinetic model was simplified to five essential reaction steps by dropping the nucleotide-induced conformational transition (step 2) and Ca^{2+} deocclusion (step 5) from Scheme 1; these two steps control the rate of the subsequent reactions, E1P formation (*36*) and E2P hydrolysis (*9, 66*), respectively. To take account of the rate control imposed by these reactions without explicitly including them in the model, E1P formation and E2P hydrolysis were assigned rate constants corresponding to the conformational transition (180−200 s^{-1}) and Ca^{2+} deocclusion (5−20 s^{-1}). A further simplification involved combining E2·P_i breakdown and the conformational transition, E2 → E1, into a single step: E2·P_i → E1 + P_i (step 5). Identical simulation results were achieved with a model that included E2·P_i breakdown and the E2 → E1 conformational transition as separate reactions; this was accomplished by assigning the individual steps rate constants consistent with the forward rate for step 5 in the simplified scheme. In that case, the rate limitation imposed by reactions following E2P hydrolysis was divided between two reactions equivalent to having only one slow reaction. Initial values for the forward and reverse rate constants were selected from the literature (*9*) or approximated as zero on the assumption that product formation is negligible.

The kinetic parameters obtained by simulation of the data in Figure 2 are summarized in Table 2. The rate constants corresponding to E2P hydrolysis (step 4) and P_i release (step 5) were selected to simulate the rise of the phosphoenzyme to its steady-state level while simultaneously matching the lag and linear phases of the time dependence of P_i liberation. Between 10 and 100 μM ATP, the simulated rate of E2P hydrolysis increased 3-fold (7−20 s^{-1}) while E2·P_i turnover rose 60−70%, consistent with allosteric activation of the rate of breakdown of these intermediate states by ATP. For both sets of data, the selection of rate constants that best simulated the burst and steady-state phase of the P_i liberation (dashed lines) resulted in a prominent phosphoenzyme overshoot which underestimated the steady-state EP level and catalytic site density by approximately 1 nmol/mg of protein. The inability to fit the steady-state EP data can be traced to the steady-state velocity of P_i production, which is not fast enough to regenerate the phosphoenzyme and prevent the decay of the overshoot. Likewise, selection of rate constants that reproduced the time course of EP formation (solid lines) resulted in an underestimation of the P_i burst amplitude by a similar amount. Because the decay of the phosphoenzyme overshoot leads to the formation of E2·P_i, anything which limits the decay of the overshoot (e.g., increasing the rate of reversal of E2P → E2·P_i) will also reduce the P_i burst amplitude. Further adjustments in these rate constants and the introduction of additional intermediate states in the reaction cycle did not improve the fit, suggesting that a simple linear consecutive scheme is inadequate for modeling the quenched-flow data in Figure 2. In addition, the mechanism as depicted has ATP entering the cycle at a single step (binding to E1) and will not accommodate the additional high-affinity effects of ATP on pre-steady-state phosphoenzyme hydrolysis and P_i release observed in these experiments. Such effects imply the existence of an additional high-affinity ATP binding site that becomes occupied in a range of ATP concentrations where phosphorylation is incompletely saturated. These characteristics (*9*), in addition to the X-ray diffraction evidence for a single nucleotide binding in the crystal structure of SERCA1 (*5*), support a model in which the high-affinity allosteric ATP binding site corresponds to the catalytic site on a neighboring subunit (*9*−*11*).

Table 2: Kinetic Constants for the Native and $C_{12}E_8$-Solubilized SR Ca-ATPase at 21 °C[a]

rate constants forward/reverse	native membranes: 10 μM ATP	native membranes: 100 μM ATP	$C_{12}E_8$-solubilized Ca-ATPase, 10 μM ATP
k_1/k_{-1}	$1.1 \times 10^7/35$	$1.1 \times 10^7/35$	$1.1 \times 10^7/35$
k_2/k_{-2}	180/0	180/0	180/0
k_3/k_{-3}	500/0	500/0	375/10
k_4/k_{-4} (—)	7/14	20/40	28/28
k_4/k_{-4} (---)	7/0	20/9.5	na
k_5/k_{-5} (—)	12/0	20/0	19/0
k_5/k_{-5} (---)	6/0	9.5/0	na
site density (nmol/mg)	4.3	4.3	2.3

[a] Phosphoenzyme formation (filled circles) and phosphate (P_i) release (open circles) in Figure 2 (native enzyme) and Figure 5 ($C_{12}E_8$-solubilized enzyme) were simulated using the rate constants shown in the table according to the scheme E1 + ATP ⟨1⟩ E1·ATP ⟨2⟩ E1P ⟨3⟩ E2P ⟨4⟩ E2·P_i ⟨5⟩ E1 + P_i (see Materials and Methods). The solid line simulations in Figure 2, which are optimal for EP formation but underestimate burst phase P_i release, were generated using either $k_4/k_{-4} = 7\ s^{-1}/14\ s^{-1}$ and $k_5/k_{-5} = 12\ s^{-1}/0$ (panel A, 10 μM ATP) or $k_4/k_{-4} = 20\ s^{-1}/40\ s^{-1}$ and $k_5/k_{-5} = 20\ s^{-1}/0$ (panel B, 100 μM ATP). The dashed line simulations in Figure 2, which are optimal for P_i release but underestimate steady-state EP formation, were generated with $k_4/k_{-4} = 7\ s^{-1}/0$ and $k_5/k_{-5} = 6\ s^{-1}/0$ (panel A, 10 μM ATP) or $k_4/k_{-4} = 20\ s^{-1}/9.5\ s^{-1}$ and $k_5/k_{-5} = 9.5\ s^{-1}/0$ (panel B, 100 μM ATP). Simulation of EP formation and P_i release in the $C_{12}E_8$-solubilized Ca-ATPase was accomplished using a single set of rate parameters. The units of k_1 are in $M^{-1}\ s^{-1}$. All other rate constants are in s^{-1}. na = not applicable.

Dephosphorylation of the Phosphoenzyme by ADP at 21 °C. Figure 3 shows ADP-induced phosphoenzyme decomposition at 21 °C after 116 ms of phosphorylation in standard buffer containing 0.1 M KCl and either 10 μM ATP (panel A) or 100 μM ATP (panel B). Dephosphorylation was initiated by the addition of either 1.66 mM ADP (filled circles) or 1.66 mM ADP + 5 mM $CaCl_2$ (filled squares) and allowed to proceed for 289 (10 μM ATP) or 542 ms (100 μM ATP) prior to quenching with acid. Similar to the behavior at 2 °C, the resulting ADP dephosphorylation pattern was triphasic with fast, intermediate, and slow decay components. Phosphate production following the addition of ADP (open circles) was closely correlated with the secondary phase of phosphoenzyme decay in terms of both its amplitude and rate. The EP decay components were analyzed as described above, and the values from the data fits are

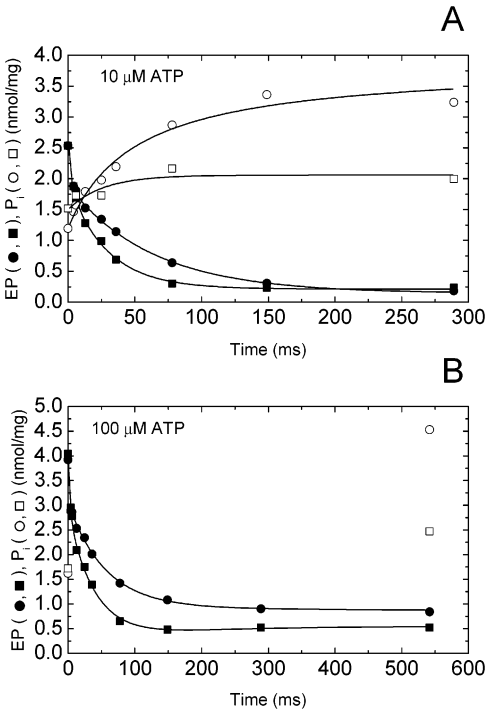

FIGURE 3: Dephosphorylation by ADP and ADP + $[Ca^{2+}]$ jump at 21 °C after 116 ms of phosphorylation in the presence of 0.1 M KCl and either 10 μM (panel A) or 100 μM [γ-^{32}P]ATP (panel B). SR vesicles (0.375 mg/mL) were phosphorylated for 116 ms in a solution containing 100 mM KCl, 5 mM $MgCl_2$, 0.45 mM $CaCl_2$, 0.5 mM EGTA (3.5 μM ionized Ca^{2+}), and 20 mM MOPS (pH 7.0). At $t = 0$, 1.66 mM ADP (circles) or 1.66 mM ADP + 5 mM $CaCl_2$ (squares) was added to initiate dephosphorylation. The reaction was terminated at the indicated times by addition of 3% perchloric acid + 2 mM H_3PO_4. Phosphoenzyme decay (closed symbols) and phosphate (P_i) release (open symbols) were measured as described in Materials and Methods. The lines represent the best fits to the data using the parameters listed in Table 3.

Table 3: ADP-Induced and ADP + Ca^{2+}-Induced Dephosphorylation of SR Ca-ATPase at 0.1 M KCl and 21 °C[a]

dephosphorylation conditions	[E1P] (nmol/mg)	k_1 (s^{-1})	[E2P] (nmol/mg)	k_2 (s^{-1})	$\Delta[P_i]$ (nmol/mg)
10 μM ATP					
1.66 mM ADP	0.53	nr	2.00	16	2.05
1.66 mM ADP + 5 mM $CaCl_2$	0.40	nr	2.15	35	0.48
100 μM ATP					
1.66 mM ADP	1.00	nr	2.00	14	2.91
1.66 mM ADP + 5 mM $CaCl_2$	1.00	nr	2.50	24	0.75

[a] The kinetic model, initial parameter values, and constraints used in fitting ADP-induced dephosphorylation in Figure 3 are given in the legend to Table 1. The fast component rate constant (k_1) was not time-resolved (nr).

summarized in Table 3. In both experiments, the E1P intermediate was a smaller fraction of the steady-state phosphoenzyme (21% E1P at 10 μM ATP and 33% E1P at 100 μM ATP) than at 2 °C (47%; Table 1). Compared to our previous measurements (*9*), the fraction of E1P measured at 10 μM ATP decreased (from 33% to 21%) while the amount of P_i release associated with E2P decay increased, achieving a 1:1 stoichiometric relationship in these experiments. The addition of 5 mM $CaCl_2$ to the dephosphorylation mixture ($[Ca^{2+}]$-jump conditions) doubled the decay rate of the intermediate component at both 10 and 100 μM ATP (Figure 3, Table 3), linking this component with E2P. Further proof of this was obtained from the corresponding time course of P_i production (open squares), which increased in rate but was reduced in amplitude compared to P_i release in the absence of the $[Ca^{2+}]$ jump.

The absence of a rapid phase of P_i production coinciding with the fast component of dephosphorylation identifies the latter as resulting from the transfer of enzyme-bound phosphate from E1P to ADP to form E1·ATP. In contrast, P_i production is quantitatively correlated with the decay of the intermediate component, implying that this component corresponds to the hydrolysis of E2P to E2 + P_i. Phosphate production during the intermediate decay phase is incompatible with the interpretation of Pickart and Jencks (*56*), who identified the fast and intermediate phases of EP decay with the transformation of E1P·ADP to E1·ATP and E1·ATP to E1 + ATP, respectively. In their quenched-flow experiments, all of the phosphoenzyme formed from acetyl phosphate was used to synthesize ATP in the presence of ADP; consequently, there was no need to identify the secondary decay phase with E2P decomposition. From the relationship of EP decay and P_i liberation in Figure 3A, the disappearance of the intermediate component corresponds to the hydrolysis of E2P to E2 + P_i (or E2·P_i) (filled circles; nonjump conditions) or to a combination of E2P hydrolysis and E1·ATP formation (filled squares; $[Ca^{2+}]$-jump conditions). Thus, jumping the $[Ca^{2+}]$ together with [ADP] opens up a second pathway for E2P decay, namely, E2P → E1P + ADP → E1P·ADP → E1·ATP. This reduces the total amount of P_i production (as a result of competition between E2P hydrolysis and E1P formation) and increases the rate of dephosphorylation (as a result of ATP synthesis from E1P·ADP).

To determine how the poise of the E1P ↔ E2P conformational equilibrium changes with the intravesicular Ca^{2+} level, ADP dephosphorylation experiments were carried out at 21 °C using tightly sealed SR vesicles passively loaded with 5 mM Ca^{2+}. SR vesicles were suspended at 0 °C for 6 h in a medium containing 50 mM KCl, 3 mM $MgCl_2$, and 40 mM MOPS, pH 6.8, either with or without 5 mM $CaCl_2$. The free $[Ca^{2+}]$ in the extravesicular medium was adjusted to ~100 μM at the time of phosphorylation by adding 5 mM EGTA to the Ca^{2+}-loaded vesicles. Free $[Ca^{2+}]$ in the control (unloaded) vesicles was adjusted to a similar level by the addition of 0.1 mM $CaCl_2$ to the enzyme medium prior to the start of phosphorylation. Figure 4 shows ADP-induced phosphoenzyme decomposition in unloaded control vesicles (filled circles) and Ca^{2+}-loaded vesicles (filled squares) following 116 ms of phosphorylation with 10 μM ATP. The Ca^{2+}-loaded vesicles exhibit fast and intermediate decay phases similar to those of the unloaded control vesicles. The contribution of E1P to EP_{total} in the Ca^{2+}-loaded vesicles was 53% compared to 31% in the unloaded control vesicles (Table 4). E2P decay in the Ca^{2+}-loaded sample, 31 s^{-1}, was increased relative to the decay rate in the control sample, 23 s^{-1}. These features, and the decrease in total P_i release associated with E2P decay in the Ca^{2+}-loaded vesicles (Figure 4, open squares), attest to the increased activity of the reverse conformational transition, E2P → E1P. High intravesicular $[Ca^{2+}]$ favors occupation of the low-affinity transport sites on E2P, preventing E2P hydrolysis following

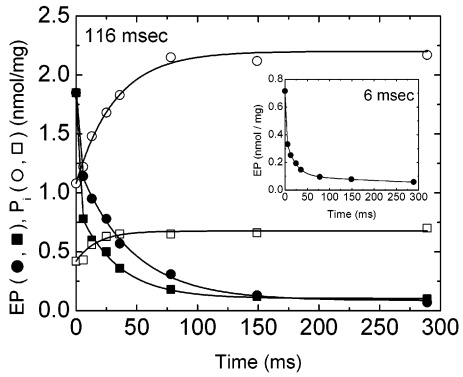

FIGURE 4: Dephosphorylation of Ca^{2+}-loaded SR vesicles by ADP at 21 °C after 116 ms (main panel) or 6 ms (inset) of phosphorylation in the presence of 0.1 M KCl. SR vesicles (0.375 mg/mL) preloaded with 5 mM $CaCl_2$ (squares) or control unloaded vesicles (circles) were phosphorylated for 116 ms by 10 μM [γ-^{32}P]ATP (as in Figure 3), after which 1.66 mM ADP (final concentration) was added, and the reaction was terminated at the indicated times by 3% perchloric acid + 2 mM H_3PO_4. Phosphoenzyme decay (filled symbols) and phosphate (P_i) release (open symbols) were measured as described in Materials and Methods. The lines represent the best fits to the data using the parameters listed in Table 4. Additional details for the experiment are provided in Materials and Methods.

Table 4: Effect of Intravesicular Ca^{2+} Loading on ADP-Induced Dephosphorylation at 0.1 M KCl and 21 °C[a]

dephosphorylation conditions	[E1P] (nmol/mg)	k_1 (s^{-1})	[E2P] (nmol/mg)	k_2 (s^{-1})	$\Delta[P_i]$ (nmol/mg)
unloaded vesicles	0.56	nr	1.23	23	1.2
Ca^{2+}-loaded vesicles	0.93	nr	0.84	31	0.38

[a] The conditions for passive loading SR Ca-ATPase vesicles with 5 mM $CaCl_2$ and for measuring ADP-induced EP decay in Figure 4 are described in Materials and Methods. The kinetic model, initial parameter values, and constraints used in fitting ADP-induced dephosphorylation in Figure 4 are given in the legend to Table 1. The fast component rate constant (k_1) was not time-resolved (nr).

Ca^{2+} release. Inhibition of E2P hydrolysis by the internal Ca^{2+} load during cycling is evident from the reduced P_i production at the time of addition of ADP ($t = 0$; Figure 4), which was only 32% of the value found in unloaded vesicles. The results in Figure 4 suggest that the E1P ↔ E2P poise is not highly sensitive to intravesicular [Ca^{2+}] and that a significant fraction of the P_i released during cycling derives from the hydrolysis of E2P, despite the high internal Ca^{2+} load tending to stabilize this intermediate. This differs from the interpretation of Yu and Inesi (*67*) and De Meis (*68*), who associate P_i production in Ca^{2+}-loaded SR vesicles with hydrolysis of the ADP-sensitive phosphoenzyme, E1P.

At 21 °C, unloaded SR membrane vesicles rapidly accumulate E2P in the pre-steady state of phosphorylation, reaching 85% of the final steady-state level 6 ms after the addition of ATP (*9*). Computer simulations revealed that the E1P → E2P transition rate in the pre-steady state has to be at least 500 s^{-1} to produce this behavior. We tested how rapidly E2P accumulates in the presence of a 5 mM intravesicular Ca^{2+} load by chasing the phosphoenzyme formed from 10 μM ATP with 1.66 mM ADP 6 ms after the start of phosphorylation. As seen in the inset to Figure 4, two components dominate the EP decay curve with a distribution of 51% fast (E1P decay) and 49% slow (E2P decay). The proportions of these decay components are very similar to those observed at 116 ms, indicating that as soon as the enzyme is phosphorylated, it very rapidly isomerizes, producing equal fractions of E1P and E2P. This behavior cannot be explained by the presence of a rapid equilibrium between E1P and E2P because that would result in a single rapid phase of EP decay when ADP is added to dephosphorylate the enzyme. The presence of the slow phase of ADP-induced EP decay following the rapid phase in Figure 4 (inset) rules out a rapid equilibrium between E1P and E2P and suggests that something else serves to stabilize E1P following its initial rapid transformation to E2P.

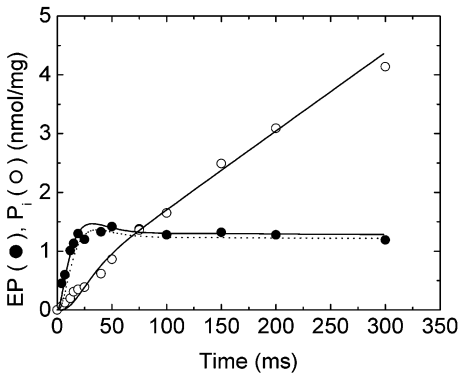

FIGURE 5: Phosphoenzyme (EP) formation and phosphate (P_i) release by the $C_{12}E_8$-solubilized Ca-ATPase at 21 °C in the presence of 0.1 M KCl and 10 μM [γ-^{32}P]ATP. The Ca-ATPase in SR vesicles was solubilized with $C_{12}E_8$ as described in Materials and Methods. The $C_{12}E_8$−Ca-ATPase (0.5 mg/mL) was phosphorylated in a solution containing 100 mM KCl, 3 mM $MgCl_2$, 1.5 mM $CaCl_2$, 1 mM EGTA, 20 mM TES (pH 7.0), 50 μM mercaptoethanol, and 5 mg/mL $C_{12}E_8$. At the indicated times the reaction was terminated by the addition of 3% perchloric acid + 2 mM H_3PO_4. Phosphoenzyme formation (filled circles) and P_i release (open circles) were measured as described in Materials and Methods. The time course of EP formation and P_i release (solid lines) was simulated using the rate constants and kinetic scheme shown in Table 2. The dashed line shows the time course of E2P formation, calculated from the ADP dephosphorylation data for the $C_{12}E_8$-solubilized Ca-ATPase shown in Figure 6 and described in the text. Additional details for the simulations are provided in the text.

Effect of $C_{12}E_8$ on the Ca-ATPase Partial Reactions at 21 °C. Solubilization of the native skeletal SR Ca-ATPase with the nonionic detergent, $C_{12}E_8$, produces a monomeric enzyme with the retention of Ca^{2+}-dependent enzymatic activity (*50*). Andersen et al. (*52*) reported that the enzymatic properties of the Ca-ATPase, including the ability to undergo the E1P → E2P conformational transition and discharge Ca^{2+} from low-affinity sites on E2P, are preserved in the presence of monomer-forming concentrations of $C_{12}E_8$. Using quenched-flow mixing, we tested whether conversion of the Ca-ATPase to a monomeric state by $C_{12}E_8$ alters its kinetic properties compared to the behavior in native SR. Native skeletal SR Ca-ATPase was solubilized with $C_{12}E_8$ at a 10:1 ratio of detergent to SR protein to generate active ATPase monomers (*52*). After removal of the insoluble residue, EP formation and P_i release from ATP were measured in a quenched-flow apparatus under conditions similar to those used in experiments with native SR membranes (see Materials and Methods). As seen in Figure 5, phosphorylation of the soluble enzyme with 10 μM ATP followed an exponential time course in the pre-steady state, reaching a maximum value within 40−50 ms. Inorganic phosphate production increased

rapidly during the initial 60−75 ms of the reaction and then slowed down as ATP hydrolysis enters the steady state. These characteristics qualitatively resemble the behavior seen in native SR membranes (Figure 2A) but differ quantitatively in showing faster initial (burst phase) and final (steady-state) rates of P_i production. In contrast to the native Ca-ATPase, simulation of phosphorylation and P_i production using a simplified linear consecutive reaction mechanism gave a reasonably good fit to the transient and steady-state experimental data (Figure 5). This is attributed to faster rates of E2P hydrolysis (28 vs 7 s^{-1}) and enzyme recycling, E2 → E1 (19 vs 12 s^{-1}), allowing rephosphorylation of the $C_{12}E_8$-solubilized Ca-ATPase to proceed more rapidly than in the native, membranous enzyme (Table 2). The transient decline in the EP level following the overshoot is also prevented by rapidly reversible E2P hydrolysis ($k_4/k_{-4} = 1$). This reversibility is also manifested in the biphasic pattern of ADP-induced E2P decay in the steady state of phosphorylation (see below), a feature not found in the native membranous enzyme (Figures 3 and 4). In contrast to the kinetics of P_i liberation, ATP binding and phosphorylation (E1P formation) have rates that are indistinguishable from those in the native Ca-ATPase (Table 2). The maximum level of phosphorylation in the soluble Ca-ATPase was roughly half that found in the native preparation, despite its prolonged stability at room temperature and the absence of formation of insoluble aggregates. The reduced activity may have resulted from an initial loss of enzyme activity during solubilization with the detergent or from sequestration of the enzyme in detergent micelles. The absence of significant changes in the kinetics of ATP binding and phosphorylation in the soluble enzyme suggests that it retains functional capabilities similar to those of the membranous enzyme. These properties are similar to those reported by Kosk-Kosicka et al. (*51*), who found lower levels of phosphorylation at less than saturating [ATP] in the $C_{12}E_8$-solubilized SR Ca-ATPase than in the membranous enzyme under similar conditions.

ADP chase experiments were carried out under pre-steady-state and steady-state conditions to determine how rapidly E1P is converted to E2P in the $C_{12}E_8$-solubilized Ca-ATPase at 21 °C. Figure 6A shows a two-stage mixing experiment in which the ADP chase (1.66 mM, final concentration) was added 6 ms after the start of phosphorylation by 10 μM ATP. As in the native enzyme, the time course of EP decomposition was triphasic with fast (unresolved), intermediate (35 s^{-1}), and slow decay (1.3 s^{-1}) components. The concentrations of the fast and intermediate decay components were identical at 0.21 nmol/mg of protein, representing 87% of EP_{total}. Adding 5 mM Ca^{2+} to the ADP chase at 6 ms increased the rate of dephosphorylation of the intermediate decay component (35 to 85 s^{-1}) without affecting the proportions of the fast and intermediate decay components (Figure 6A, Table 5). The absence of data points in the fast decay component and [Ca^{2+}]-jump sensitivity of the intermediate component distinguish these as E1P and E2P, respectively. When ADP was added after 116 ms of phosphorylation (steady state, Figure 5B), E1P was reduced to ~6% of the phosphoenzyme in the main catalytic pathway, down from 50% at 6 ms, while E2P rose from 50% to 94% (Table 5). Thus, the principal phosphorylated intermediates of the reaction cycle, E1P and E2P, behave like consecutive intermediates in the $C_{12}E_8$-solubilized Ca-ATPase. Phosphoenzyme decay at 116 ms was stoichiometric with P_i release (Figure 6B), consistent with accumulation of the steady-state phosphoenzyme in E2P. In contrast to the native enzyme, ADP-induced E2P decomposition was biphasic with roughly equal amounts of phosphoenzyme in the fast (50 s^{-1}; 0.43 nmol/mg) and slow decay phases (13 s^{-1}; 0.33 nmol/mg) (Table 5). This decay pattern is consistent with a two-step

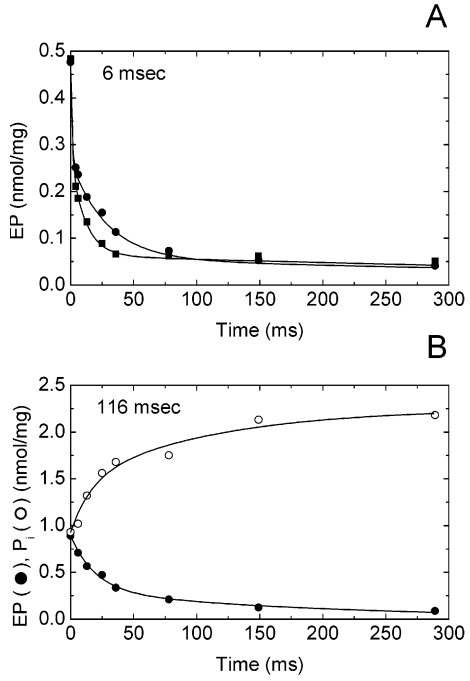

FIGURE 6: Phosphoenzyme decomposition of $C_{12}E_8$-solubilized Ca-ATPase in the presence of 0.1 M KCl at 21 °C following the addition of ADP or ADP + Ca^{2+} ([Ca^{2+}] jump) to SR vesicles phosphorylated for 6 ms (panel A) or 116 ms (panel B). The Ca-ATPase in SR vesicles was solubilized with $C_{12}E_8$ as described in Materials and Methods and phosphorylated with 10 μM [γ-^{32}P]-ATP as described in the legend of Figure 5. After 6 or 116 ms of phosphoenzyme formation, either (filled circles) 1.66 mM ADP or (filled squares) 1.66 mM ADP + 5 mM $CaCl_2$ (final concentrations) was added, and the reaction was terminated at the indicated times by the addition of 3% perchloric acid + 2 mM H_3PO_4. In the dephosphorylation experiment using $C_{12}E_8$-solubilized Ca-ATPase phosphorylated for 116 ms (panel B), inorganic phosphate (P_i) liberation (open circles) following the addition of 1.66 mM ADP was also measured. The lines represent the best fits of the data using the parameters listed in Table 5.

Table 5: Effect of $C_{12}E_8$ Solubilization on ADP-Induced Dephosphorylation at 0.1 M KCl and 21 °C[a]

dephosphorylation conditions	[E1P] (nmol/mg)	k_1 (s^{-1})	[E2P] (nmol/mg)	k_2 (s^{-1})	[E2P] (nmol/mg)	k_3 (s^{-1})	Δ[P_i] (nmol/mg)
6 ms							
1.66 mM ADP	0.21	nr	0.21	35	0	0	nd
1.66 mM ADP + 5 mM $CaCl_2$	0.21	nr	0.21	88	0	0	nd
116 ms							
1.66 mM ADP	0.05	nr	0.43	50	0.33	13	1.25

[a] The conditions for $C_{12}E_8$ solubilization of the Ca-ATPase and for measuring ADP-induced EP decay in Figure 6 are described in Materials and Methods. The kinetic model, initial parameter values, and constraints used in fitting ADP-induced dephosphorylation in Figure 6 are given in the legend to Table 2 and described in the text. The fast component rate constant (k_1) was not time-resolved (nr). Inorganic phosphate production during ADP dephosphorylation was not determined (nd) for the 6 ms experiment.

reaction mechanism involving a rapidly reversible hydrolytic reaction, E2P ↔ E2·P_i, followed by slow P_i release from E2·P_i. These conditions satisfy the requirements for simulation of P_i production in the single-mix quenched-flow experiment in Figure 5, in which rapidly reversible E2P hydrolysis ($k_4 = k_{-4} = 28$ s^{-1}) precedes slow (19 s^{-1}) P_i release from E2·P_i. The absence of biphasic E2P decay kinetics in the native membranous enzyme implies that the E2P hydrolysis in that system is not highly reversible. Consequently, the high steady-state phosphorylation activity and absence of a prominent overshoot likely involves some other feature of the catalytic mechanism in the native enzyme as suggested by the simulations in Figure 2.

From the proportions of E2P present in the soluble enzyme after 6 (50%) and 116 ms (96%) of phosphorylation by ATP, we were able to reproduce the time course of E2P formation shown in Figure 5 (dashed line simulation) using the conventional linear consecutive (monomeric) reaction scheme. The rate constant for the E1P → E2P transition obtained from this simulation was 375 s^{-1}, less than the rate constant for the conformational transition in native permeabilized SR vesicles (>500 s^{-1}; ref *9*) and much less than the transition rate in Ca^{2+}-loaded vesicles. In the latter system, a constant ratio of phosphorylated intermediates is established within the first 6 ms as evidenced by the lack of a significant change in the fraction of E2P between 6 (49%) and 116 ms (47%) (Table 5). We conclude that the smaller transition rate constant in the soluble monomeric enzyme reflects the loss of oligomeric structure essential for mediation of the allosteric effects of ATP and free energy exchange between the subunits.

DISCUSSION

In the present study, quenched-flow mixing was used to characterize the kinetic and thermodynamic behavior of the phosphorylated intermediates in the catalytic cycle of the sarcoplasmic reticulum (SR) Ca-ATPase (SERCA1). Experiments were carried out at 2 °C to match the conditions of an earlier study (*12*) in which transient EPR signals from iodoacetamide spin-labeled (IASL) Ca-ATPase were measured following a laser flash-induced [ATP] jump and correlated with measurements of EP formation and P_i release. An advantage of working at the reduced temperature is that it provides information on the initial formation of phosphorylated intermediates, which was not well-resolved in our previous experiments at 21 °C (*9*). A separate series of quenched-flow measurements was carried out at 21 °C for comparison with the results obtained at 2 °C. Both sets of measurements exclude a simple linear consecutive model as a plausible explanation for the catalytic properties of the skeletal Ca-ATPase in native SR membranes. In contrast, this model will accommodate the kinetic features of the $C_{12}E_8$-solubilized SR Ca-ATPase, which is monomeric under our experimental conditions.

We previously reported (*12*) that the time course of phosphorylation at 2 °C is biphasic, in agreement with the earlier studies of Ikemoto et al. (*13*, *15*). In contrast, the corresponding transient EPR spectrum of iodoacetamide spin-labeled CaATPase (*44*), resulting from the accumulation of a restricted mobility component, was monophasic after a brief lag phase and correlated with the slow phase of phosphorylation over a wide range of salt concentrations (0−0.6 M KCl). ADP chase experiments conducted at 2 °C (present study) showed that the amount of E1P produced during the fast phase of phosphorylation is a small fraction (2%) of the total EP (Table 1), implying that E1P turns over rapidly (>500 s^{-1}), even at reduced temperatures. This might explain the absence of the fast EPR transient during the initial stages of phosphorylation because the signal-producing E1P intermediate (*12*, *48*) is very unstable. The more slowly decaying component following the ADP-sensitive phase was [Ca^{2+}]-jump sensitive; i.e., it disappeared more rapidly in response to mixing with 1.66 mM ADP and 5 mM $CaCl_2$ than with ADP alone (Figure 1, Table 1). The [Ca^{2+}]-jump sensitivity of the slow decay component distinguishes it as being ADP-insensitive E2P, which contains low-affinity transport (release) sites for Ca^{2+}. At longer phosphorylation times, the fraction of E1P *increased*, eventually equaling one-half of the total acid-stable intermediate pool (Table 1). This behavior is reversed from the sequence of events in Scheme 1, which predicts that the proportion of E1P should be maximal during the initial stages of phosphorylation and should *decrease* as it becomes converted to E2P at longer reaction times.

The absence of significant levels of E1P (fast phase of ADP-induced dephosphorylation) at 6 and 10 ms in Figure 1 could result from a slow rate of ADP dissociation from E1P·ADP, rendering the latter insensitive to added ADP in the chase. To resolve this question, we need to consider two interpretations of the mechanism of dephosphorylation of E1P by ADP. In the first of these we shall assume that the fast phase of dephosphorylation of the Ca-ATPase is an aspect of its normal catalytic behavior. In that situation the rapid disappearance of E1P induced by ADP reflects the presence of a very rapid rate of reversal of phosphorylation, which was not resolved in these experiments. If E1P decay is virtually (99%) complete by the first data point following the addition of ADP (4 ms), then the rate of formation of E1·ATP from E1P·ADP, τ, must be at least 1200 s^{-1}, where τ equals the sum of the forward and reverse constants for phosphorylation, $k_f + k_r$. k_f is unknown because the rate of phosphorylation at 2 °C, 70−80 s^{-1}, is rate-limited by the conformational transition preceding phosphorylation (step 2, Scheme 1). We argue below that the EP species remaining after the fast decay at 116 ms (Figure 1C) is E2P on the basis of its [Ca^{2+}]-jump sensitivity. If E1P disappears stoichiometrically following the ADP chase, i.e., if all that remains is E2P, then the reverse rate constant for phosphorylation must be similar to τ ($k_r \sim 1000$ s^{-1}). Because reversal of phosphorylation competes with ADP dissociation from E1P·ADP, ADP dissociation must be faster than the estimated rate of reversal (>1000 s^{-1}) to account for the high levels of phosphorylation measured in these experiments (∼50% of total site density). Such a high rate of ADP dissociation would lead to the rapid formation of E1P from E1P·ADP, rendering this phosphoenzyme immediately sensitive to ADP in the chase. Even if E1P·ADP exists in a quasi-equilibrium with E1·ATP following the ADP chase as proposed by Pickart and Jencks (*55*), k_r must be ∼600 s^{-1} to account for the 50% of EP remaining after the rapid phase of dephosphorylation. Consequently, the inability to detect E1P at 10 ms cannot result from the slow dissociation of ADP from E1P·ADP *if* ADP-induced dephosphorylation of E1P occurs with a rate constant ≥1200 s^{-1}.

Another possibility is that rapid dephosphorylation induced by ADP is not a normal feature of catalysis but results instead from a chemical transformation in the protein occurring after acid denaturation. This might involve the migration of covalently bound phosphate from Asp-351 to bound ADP during acid denaturation of the pump protein following the addition of the quench:

$$E1P(Ca_2)\cdot ADP \xrightarrow{H^+} E1(Ca_2)\cdot ATP$$

This would take place immediately after the acid quench is added and before denaturation of the pump protein releases ADP from its binding site on the N domain. We assume that this reaction is stoichiometric and irreversible, so that none of the E1P·ADP formed as a consequence of phosphorylation (E1·ATP → E1P·ADP) or ADP binding to the phosphoenzyme (E1P + ADP → E1P·ADP) *prior* to the quench escapes detection after being mixed with ADP. The saturating concentration of ADP used in the chase solution ensures that the formation of E1P·ADP is quantitative with the level of E1P that accumulates before acid quenching. Moreover, because this transformation occurs after quenching of the catalytic reaction, there is no record of its time dependence in the ADP-induced decay curve (Figure 1). Thus, dephosphorylation of E1P in the ADP chase experiment appears to be instantaneous but may actually require several milliseconds to reach completion after quenching with acid. We conclude that *if* the unresolved decay of ADP-sensitive E1P is caused by the acid-induced transmigration of phosphate from the catalytic site to bound ADP, then the failure to detect significant formation of E1P during the initial stages of phosphorylation must result from its very rapid (enzyme-catalyzed) conversion to E2P.

It is noteworthy that the phosphorylated Na,K-ATPase from eel electric organ shows similar behavior in response to chasing with ADP (*14*) but that ADP-induced dephosphorylation of the chymotrypsin-digested pig kidney Na,K-ATPase can be resolved with a rate constant of ~200 s^{-1} (*69*). Partial chymotryptic digestion, which blocks the conversion of E1P to E2P in Na,K-ATPase (*70*) and in skeletal SR Ca-ATPase (*71*), may alter the intramolecular interactions involving the N, P, and A domains in the pump protein after ADP binding. Nucleotide-induced movement of the N domain toward the P domain occurs prior to catalytic site phosphorylation in SERCA1 (*8*), and modulation of that movement by the A domain might have a role in transferring phosphate from the catalytic site (P domain) to bound ADP (N domain) after quenching.

The arguments for the rapid conversion of E1P to E2P at 2 °C rest on the assumption that the decay phase immediately following the disappearance of E1P represents decomposition of the ADP-insensitive phosphoenzyme, E2P. At 21 °C, this interpretation is supported by the fact that P_i production in unloaded vesicles shows a similar rate and stoichiometry to EP turnover in the intermediate phase (Figure 3). In addition, turnover of the intermediate decay component is accelerated by jumping the Ca^{2+} concentration in conjunction with ADP, reflecting reversal of the conformational transition and the resynthesis of ATP following Ca^{2+} binding to the low-affinity sites on E2P. At 2 °C, P_i production was negligible after chasing with ADP (Figure 1C), and we had to rely on the [Ca^{2+}]-jump sensitivity of the intermediate decay to positively correlate it with E2P breakdown. Although we assume that sensitivity to the [Ca^{2+}] jump arises from occupation of the low-affinity transport sites on E2P, access to those sites might not be restricted to the luminal membrane surface as suggested by our earlier measurements in the absence of ionophore (*9*). Those experiments demonstrated that Ca^{2+} binds from the extravesicular surface of the membrane, implying that the transport sites become available as a consequence of spontaneous reorientation or by a conformational change induced by the interaction of E2P with ADP. In support of the latter explanation, additional measurements conducted with Ca^{2+}-loaded vesicles in the absence of ADP showed that turnover was inhibited from the luminal surface (*9*), in agreement with the diminished zero-time P_i production in Figure 4 (this study). P_i production in Ca^{2+}-loaded vesicles following the ADP chase is not stoichiometeric with the intermediate phase of EP decay in Figure 4, suggesting that Ca^{2+} inside the vesicle stimulates ATP resynthesis by binding to E2P and activating reversal of the conformational transition. We conclude that the [Ca^{2+}]-jump sensitivity of the intermediate decay phase is caused by occupation of the low-affinity transport sites on E2P, albeit this can occur from both the extravesicular and luminal directions. Reorientation of these sites (from the luminal to the extravesicular surface) results from a conformational change in E2P induced by ADP binding. Exposure of these sites to opposite sides of the membrane must take place sequentially (rather than simultaneously); otherwise, depletion of the transport gradient would occur, preventing ATP synthesis coupled to pump reversal (*72*). The alternative to this explanation assumes that another species is responsible for the intermediate decay at 2 °C and that the similarity of this behavior to the pattern of ADP-induced decay at 21 °C is coincidental. The possibility that the intermediate phase reflects ATP dissociation from E1·ATP as suggested by Pickart and Jencks (*56*) seems unlikely because E1·ATP contains high-affinity binding sites that are already occupied by Ca^{2+}, preventing a further increase in saturation by jumping the [Ca^{2+}].

The rapid appearance of E2P and delayed accumulation of E1P demonstrated in these ADP chase experiments (Figure 1) are difficult to reconcile with the linear consecutive mechanism (Scheme 1) used to interpret the SR Ca-ATPase. In this scheme, adapted from the Albers−Post model of the Na,K-ATPase, E1P and E2P are consecutive intermediates, requiring that E1P accumulate initially and then decline as E2P increases. The reverse pattern (i.e., rapid accumulation of E2P followed by a slow buildup of E1P) observed in these experiments could arise from an isomerization reaction that strongly favors E2P and is driven back toward E1P as sequestered Ca^{2+} rebinds to the low-affinity transport sites on E2P. This possibility was excluded in the present study by employing conditions that prevented significant intravesicular Ca^{2+} accumulation, namely, short reaction times, low temperatures, and permeabilization of the vesicles with the Ca^{2+} ionophore A23187. We conclude that the unusual pattern of accumulation of the ADP-sensitive and ADP-insensitive intermediates at 2 °C cannot be attributed to a time-dependent shift in the E1P ↔ E2P equilibrium toward E1P and that some other mechanism is responsible for this behavior.

The failure of linear consecutive schemes to explain qualitative features of the kinetic behavior of the skeletal

Scheme 2

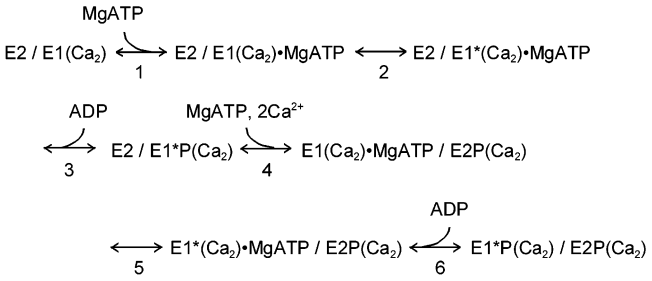

SR Ca-ATPase at 2 and 21 °C justifies consideration of alternative mechanisms involving parallel pathways of phosphorylation. In these models, the pathways may operate independently, as in isozymes or posttranslationally modified enzymes, or they may communicate via conformational coupling, which is characteristic of oligomers (*9*, *14*). Oligomeric coupling can lead to staggering of the catalytic reactions such that the subunits in the oligomer are one reaction step out of phase with each other during cycling (*9*, *13*, *15*). In our experiments at 2 °C we observed that E1P accumulation is delayed with respect to E2P formation and that the steady-state ratio of phosphorylated intermediates, [E1P]/[E2P], is close to 1. This behavior suggests a Ca-ATPase dimer in which intersubunit conformational interactions allow one subunit to form E1P ahead of its neighbor; this intermediate is rapidly (>500 s^{-1}) converted to E2P, the predominant acid-stable intermediate during the initial stages of phosphorylation (Figure 1A,B). The second subunit, which is delayed relative to the first by conformational coupling, forms E1P which interacts with E2P on the first subunit, producing the stable asymmetric intermediate, E1P/E2P. The mechanism shown in Scheme 2 incorporates these events. In this scheme the starred states [E2/E1*(Ca_2)•MgATP, E2/E1*P(Ca_2)] refer to intermediates with a restricted mobility EPR signal (*12*). For this discussion, the first subunit phosphorylated (right-hand subunit) is defined as the leading subunit and its neighbor (left-hand subunit) the delayed subunit. Only half of the subunits bind Ca^{2+} at the start of the cycle because the delayed subunit is initially present in the low-affinity, E2 conformational state. This model of Ca^{2+} binding is based on a maximum equilibrium binding capacity of 8 nmol of Ca^{2+}/mg of SR protein (*64*), the presence of two Ca^{2+} binding sites per polypeptide chain in the crystal structure of SERCA1 (*4*), and a maximum enzyme site density of 7 nmol/mg of SR protein in isolated SR vesicles (*10*, *12*). A strong conformational interaction between the asymmetric subunits in E2/E1(Ca_2) prevents E2 from becoming E1(Ca_2) by a mass action effect of high-affinity Ca^{2+} binding. The remaining half of subunits are not available to bind Ca^{2+} until a transformation in the leading subunit signals their appearance. MgATP binding to the leading subunit (step 1) generates the fast (70−80 s^{-1} at 2 °C) phase of phosphorylation, which is rate-controlled by step 2 involving isomerization of the Michaelis complex. To maintain the asymmetrical E1/E2 coupling relationship in the dimer, the E1P → E2P transition following phosphorylation of the leading subunit is coupled to the E2 → E1 transition in the delayed subunit. This arrangement allows MgATP binding to the unoccupied nucleotide site on the delayed subunit to accelerate the E1P → E2P transition by driving the E2 → E1 transition toward the high-affinity E1 conformation. This explains the rapid (>500 s^{-1}) accumulation of E2P in the pre steady state at 2 °C (Figure 1) and the slower transition rate constant in the monomeric, $C_{12}E_8$-solubilized Ca-ATPase which is uncoupled from its neighbors (see below). For simplicity, MgATP and Ca^{2+} binding to the delayed subunit is represented by a single reaction (step 4), whereas the availability of new high-affinity Ca^{2+} binding sites requires that MgATP bind first and activate the E2 → E1 transition. Ca^{2+} sequestration by the delayed subunit following this transition depends on the kinetics of phosphorylation in step 6, which is rate-limited by the slow (3−4 s^{-1}) isomerization reaction (step 5) preceding it. The predicted effect on Ca^{2+} accumulation in the delayed subunit is consistent with the results of rapid mixing EGTA quench experiments (*15*) in which ATP-dependent $^{45}Ca^{2+}$ accumulation exhibited rapid and slow exponential phases in the pre-steady state at 2−4 °C. The positive correlation between the slow phases of phosphorylation and Ca^{2+} sequestration is strengthened by the fact that they show a similar reduction in rate as the [KCl] is raised (*12*, *13*).

Compared to the leading subunit, the E1P → E2P conformational transition in the delayed subunit is significantly slower as a consequence of the formation of the asymmetric dimer, E1*P(Ca_2)/E2P(Ca_2). The presence of this species is attributed to out-of-phase coupling of the catalytic reactions in the interacting subunits and is consistent with the equimolar steady-state concentrations of E1P and E2P at 2 °C (Figure 1C). Loss of quaternary protein interactions destabilizes this intermediate, resulting in the rapid turnover (375 s^{-1}) and low steady-state level of E1P measured in the $C_{12}E_8$-solubilized Ca-ATPase (Figure 6B). The highly stable nature of the E1P(Ca_2)/E2P(Ca_2) intermediate in the native enzyme arises from coupling the fast conformational transition to slow E2P hydrolysis (0.22 s^{-1} at 2 °C; ref *12*), which controls the rate of turnover of this intermediate. Before hydrolysis can take place, Ca^{2+} is released from the leading subunit by slow deocclusion from E2P(Ca_2). The association of occluded Ca^{2+} with E2P is inferred from the discrepancy between the slow kinetics of Ca^{2+} release into arsenazo-loaded SR vesicles at 2 °C (*65*) and the very rapid formation of E2P as measured in these experiments (Figure 1A,B). These steps are depicted in the following sequence representing a continuation of Scheme 2:

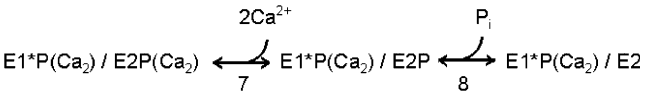

The product of the final step is identical to the product of step 3 following a symmetry operation that exchanges the positions of the subunits in the oligomer. Because the corresponding states on the adjacent subunits are structurally identical, the cycle repeats itself following P_i release from the leading subunit as the product of step 8 reenters the cycle as the precusor to step 4. Excluding Ca^{2+} binding, which occurs in the preincubation, there are three reactions that define the pre-steady-state phase of the cycle (steps 1−3) and four reactions (five if MgATP and Ca^{2+} at step 4 are treated as separate reactions) that make up the steady-state phase of this cycle.

Investigations correlating EPR spectral data from the iodoacetamide spin-labeled Ca-ATPase with intermediates

in the reaction cycle (*12*, *48*) have associated the restricted mobility EPR signal with the starred (*) states in Scheme 2. Phosphoenzyme isomerization coincides with a loss of this restricted component (E2P states do not produce this signal; ref *48*). Consequently, the starred states in the leading subunit will produce low-amplitude EPR signals if their turnover rates substantially exceed their rates of formation. Because phosphorylation of the fast phase has a rate of 70 s^{-1}, turnover of E1P on the leading subunit must be 5−10 times faster to escape early detection. The pre-steady-state ADP chase data fulfill this condition in showing little or no E1P accumulation (<5% of EP_{total}) during the initial stages of phosphorylation (6 and 10 ms; Figure 1A,B). Slow accumulation of E1P on the lagging subunit, stabilized by its interaction with E2P on the leading subunit, is expected to produce an EPR signal with similar kinetics. The kinetics of the slow EPR transient vary as a function of the [KCl], suggesting that step 5 in Scheme 2, which controls phosphorylation of the lagging subunit, is a K^+-sensitive reaction. Additional quenched-flow studies at elevated K^+ levels may shed further light on this mechanism.

There are quantitative features of the experimental results that argue against the Ca-ATPase dimer model as presented in Scheme 2. First, the dimer requires equimolar amounts of the fast and slow phases of phosphorylation to be present to account for labeling of the leading and delayed subunits. At 2 °C, this situation is realized in the presence of 0.4 M KCl (*12*, *15*), but not at 0.1 M KCl, where the ratio is 5 fast:1 slow (*12*). Second, at 2 °C, the phosphorylated enzyme (3.7 nmol/mg of protein) represents only half of the total enzyme site density in the SR membranes (6−7 nmol/mg; ref *12*). This suggests that the oligomer is larger than a dimer, possibly a trimer or a tetramer. The remaining unphosphorylated sites may be in the E2 conformation, or they may be present as a Michaelis complex, E1·ATP, and/or E2·ATP (at high ATP concentrations). Additional support for something larger than a dimer derives from our unsuccessful attempts to simulate the quantitative behavior of the pre-steady-state P_i burst and EP formation following the overshoot at 21 °C (Figure 2). This problem does not arise in the $C_{12}E_8$-solubilized enzyme (Figure 5) because rapid recycling (E2 → E1) allows the enzyme to rapidly rephosphorylate and avoid becoming trapped in E2. The constraint imposed by slow recycling of the native enzyme can be circumvented by allowing rephosphorylation to immediately follow dephosphorylation prior to completion of the reaction cycle. This will regenerate the acid-stable phosphoenzyme as it dephosphorylates to P_i, preventing the overshoot from decaying. This cannot occur in a linear reaction scheme because rephosphorylation (E1·ATP → E1P + ADP) is separated from dephosphorylation (E2P → E2 + P_i) by at least one additional step (E2 → E1); however, it can take place in an oligomer where E1P formation on one subunit is directly coupled to E2P hydrolysis on another. To maintain this coupling relationship and similar proportions of E1P and E2P in the steady state, the oligomer should have at least three subunits corresponding to the intermediate states E1P, E2P, and E2. A fourth subunit, representing the E1 state, would enable high-affinity ATP binding to activate E2P hydrolysis as observed in the pre-steady-state P_i burst (Table 2; ref *10*) and P_i ↔ HOH ^{18}O exchange (*34*) at micromolar ATP concentrations. These features are depicted in the mechanism:

$$[\text{E1}\cdot\text{ATP/E1P/E2P/E2}] + \text{ATP} \rightarrow [\text{E1P/E2P/E2/E1}\cdot\text{ATP}] + P_i + \text{ADP}$$

where each of the subunits in the oligomer (shown in brackets) proceeds to the next intermediate state in the reaction cycle coupled to the hydrolysis of one molecule of ATP. The stoichiometric equivalence of E1P and E2P predicted by this model is present at 2 °C (Figure 1C) but does not occur at 21 °C except in Ca^{2+}-loaded SR vesicles (Figure 4). The larger fraction of E2P in the unloaded vesicles at the higher temperature (Figures 3 and 4) may be due to the presence of monomers, which maintain higher steady-state levels of E2P (Table 5, Figure 6B). High luminal Ca^{2+} may help in stabilizing the oligomer which, in turn, may help to sustain the transport gradient by enhancing Ca^{2+} uptake, preventing Ca^{2+} efflux, or both.

The importance of intermolecular contacts in stabilizing E1P is evident from its virtual disappearance from the $C_{12}E_8$-solubilized enzyme under steady-state conditions (Figure 6B). The low steady-state levels of E1P in the soluble enzyme (∼6%) reflect an inherently fast turnover rate of this intermediate under conditions where oligomerization with E2P is prevented. In contrast to the steady-state distribution, about one-half of the pre-steady-state phosphoenzyme is E1P (ca. 50%; Figure 6A) as expected for the case in which E1P and E2P are consecutive intermediates. Using the conventional (monomeric) model, simulation of the E1P → E2P transition in the $C_{12}E_8$-solubilized Ca-ATPase with a forward rate constant of 375 s^{-1} and a reverse rate constant of 10 s^{-1} closely approximated the levels of E2P formation measured at 10 and 116 ms (dashed line, Figure 5). In the native Ca-ATPase, the rate of conversion of E1P to E2P is initially very fast (>500 s^{-1}) but becomes much slower in the steady state (∼10 s^{-1}), resulting in the accumulation of E1P (*9*). Solubilization of SERCA1 into monomers eliminates this behavior and yields a transition rate that is invariant with time. Our ability to model the kinetic behavior of the soluble enzyme with a conventional (Albers−Post) scheme demonstrates congruity with monomeric enzyme catalysis. Conversely, the deceleration of the E1P → E2P conformational transition and the (apparent) reversed order of formation of the phosphorylated intermediates in the native SR Ca-ATPase are inconsistent with the monomeric scheme, lending support to the hypothesis that oligomeric conformational interactions participate in these effects.

In summary, our analysis of the kinetic behavior of the native membranous SR Ca-ATPase measured over a wide range of experimental conditions argues against the Albers−Post mechanism (and other linear consecutive schemes) as a *sufficient* description of the system. Instead, the data support an oligomeric model in which the subunits communicate via conformational interactions between two, three, and possibly four subunits depending on the temperature and luminal Ca^{2+} concentration. These interactions modify the kinetic behavior so that rate constants *appear* to be time-dependent and the sequence of formation of intermediates *appears* to be reversed. These conformational interactions are likely to be strongest in asymmetric oligomers in which high (e.g., E1P)

and low (e.g., E2P) energy states are paired. The pairing of states with unequal chemical energy is a necessary condition for intersubunit free energy exchange. During cycling of the Ca-ATPase, oligomerization mediating free energy transfer between the protomers can, in principle, enhance the activity of forward reactions and/or reduce the activity of reverse reactions. These effects are expected to enhance the vectorial operation of the Ca^{2+} pump and may be an essential feature of the mechanism of energy transduction used in uphill Ca^{2+} transport.

APPENDIX

The differential equations describing the kinetic model of eq 4 are as follows:

$$d[E1]/dt = k_5[E2{\cdot}P_i] + k_{-1}[E1{\cdot}ATP] - (k_1[ATP] + k_{-5})[E1]$$

$$d[E1{\cdot}ATP]/dt = k_1[E1][ATP] + k_{-2}[E1P][ADP] - (k_2 + k_{-1})[E1{\cdot}ATP]$$

$$d[E1P]/dt = k_2[E1{\cdot}ATP] + k_{-3}[E2P] - (k_3 + k_{-2})[ADP][E1P]$$

$$d[E2P]/dt = k_3[E1P] + k_{-4}[E2{\cdot}P_i] - (k_4 + k_{-3})[E2P]$$

$$d[E2{\cdot}P_i]/dt = k_4[E2P] + k_{-5}[E1][P_i] - (k_5 + k_{-4})[E2{\cdot}P_i]$$

$$d[ADP]/dt = k_2[E1{\cdot}ATP] - k_{-2}[E1P][ADP]$$

$$d[P_i]/dt = k_5[E2{\cdot}P_i] - k_{-5}[E1][P_i]$$

The total enzyme concentration, $[E_{total}]$, is related to the sum of the concentrations of the intermediates by the conservation equation:

$$[E_{total}] = [E1] + [E1{\cdot}ATP] + [E1P] + [E2P] + [E2{\cdot}P_i]$$

At $t = 0$ (initial conditions), $[E_{total}](0) = [E1]$; all others are 0.

REFERENCES

1. Clarke, D. M., Loo, T. W., Inesi, G., and MacLennan, D. H. (1989) *Nature 339*, 476−478.
2. Ogawa, H., Stokes, D. L., Sasabe, H., and Toyoshima, C. (1998) *Biophys. J. 75*, 41−52.
3. Inesi, G., Lewis, D., Nikic, D., and Kirtley, M. E. (1992) in *Advances in Enzymology* (Meister, A., Ed.) pp 185−215, John Wiley and Sons, New York.
4. Toyoshima, C., Nakasako, M., Nomura, H., and Ogawa, H. (2000) *Nature 405*, 647−655.
5. Toyoshima, C., and Nomura, H. (2002) *Nature 418*, 605−611.
6. Andersen, J. P. (1989) *Biochim. Biophys. Acta 988*, 47−72.
7. McIntosh, D. B. (1998) *Adv. Mol. Cell Biol. 23A*, 33−99.
8. McIntosh, D. B. (2000) *Nat. Struct. Biol. 7*, 532−535.
9. Froehlich, J. P., and Heller, P. F. (1985) *Biochemistry 24*, 126−136.
10. Froehlich, J. P., and Taylor, E. W. (1975) *J. Biol. Chem. 250*, 2013−2021.
11. Froehlich, J. P., and Taylor, E. W. (1976) *J. Biol. Chem. 252*, 2307−2315.
12. Mahaney, J. E., Froehlich, J. P., and Thomas, D. D. (1995) *Biochemistry 34*, 4864−4879.
13. Ikemoto, N., Miyao, A., and Kurobe, Y. (1981b) *J. Biol. Chem. 256*, 10809−10814.
14. Froehlich, J. P., Taniguchi, K., Fendler, K., Mahaney, J. E., Thomas, D. D., and Albers, R. W. (1997) *Ann. N.Y. Acad. Sci. 834*, 280−296.
15. Ikemoto, N., Garcia, A. M., Kurobe, Y., and Scott, T. L. (1981a) *J. Biol. Chem. 256*, 8593−8601.
16. Martonosi, A., Lagwinska, E., and Oliver, M. (1974) *Ann. N.Y. Acad. Sci. 227*, 549−567.
17. Nakamura, J., and Furukohri, T. (1994) *J. Biol. Chem. 269*, 30818−30821.
18. Nakamura, J., Tajima, G., Sata, C., and Furukohri, T. (2002) *J. Biol. Chem. 277*, 24180−24190.
19. Froehlich, J. P., Bamberg, E., Kane, D. J., Clarke, R. J., Mahaney, J. E., and Albers, R. W. (2000) in *Na/K-ATPase and Related ATPases* (Taniguchi, K., and Kaya, S., Eds.) pp 349−356, Elsevier, Amsterdam.
20. Vanderkooi, J. M., Ierokomas, A., Nakamura, H., and Martonosi, A. (1977) *Biochemistry 16*, 1262−1267.
21. Papp, S., Pikula, S., and Martonosi, A. (1987) *Biophys. J. 51*, 205−220.
22. Bigelow, D. J., Squier, T. C., and Inesi, G. (1992) *J. Biol. Chem. 267*, 6952−6962.
23. Vanderkooi, J. M., Papp, S., Pikula, S., and Martonosi, A. (1988) *Biochim. Biophys. Acta 957*, 230−236.
24. Birmachu, W., and Thomas, D. D. (1990) *Biochemistry 29*, 3904−3914.
25. Quinn, P. J., Yang, L., McStay, D., Lopina, O. D., Rubtsov, A. M., and Boldyrev, A. A. (1994) *Biochem. Soc. Trans. 22*, 383S.
26. Napier, R. M., East, J. M., and Lee, A. G. (1987) *Biochim. Biophys. Acta 903*, 365−373.
27. Squier, T. C., Hughes, S. E., and Thomas, D. D. (1988) *J. Biol. Chem. 263*, 9162−9170.
28. Squier, T. C., and Thomas, D. D. (1988) *J. Biol. Chem. 263*, 9171−9177.
29. Negash, S., Chen, L. T., Bigelow, D. J, and Squier, T. C. (1996) *Biochemistry 35*, 11247−11259.
30. Martonosi, A. N. (1995) *Biosci. Rep. 15*, 263−281.
31. Kutchai, H., Mahaney, J. E., Geddis, L. M., and Thomas, D. D. (1994) *Biochemistry 33*, 13208−13222.
32. Inesi, G., Goodman, J. J., and Watanabe, S. (1967) *J. Biol. Chem. 242*, 4637−4643.
33. Yamamoto, T., and Tonomura, Y. (1967) *J. Biochem.* (*Tokyo*) *62*, 558−575.
34. McIntosh, D. B., and Boyer, P. D. (1983) *Biochemistry 22*, 2867−2875.
35. McIntosh, D. B., Clausen, J. D., Wooley, D. G., MacLennan, D. H., Vilsen, B., and Andersen, J. P. (2003) *Ann. N.Y. Acad. Sci. 986*, 101−105.
36. Petithory, J. R., and Jencks, W. P. (1986) *Biochemistry 25*, 4493−4497.
37. Suzuki, H., Obara, M., Kuwayama, H., and Kanazawa, T. (1987) *J. Biol. Chem. 262*, 15448−15456.
38. Suzuki, H., Obara, M., and Kanazawa, T. (1989) *J. Biol. Chem. 264*, 920−927.
39. Obara, M., Suzuki, H., and Kanazawa, T. (1988) *J. Biol. Chem. 263*, 3690−3697.
40. Kubo, K., Suzuki, H., and Kanazawa, T. (1990) *Biochim. Biophys. Acta 1040*, 251−259.
41. Lewis, S. M., and Thomas, D. D. (1991) *Biochemistry 30*, 8331−8139.
42. Coan, C., and Inesi, G. (1977) *J. Biol. Chem. 252*, 3044−3049.
43. Coan, C., Verjovski-Almeida, S., and Inesi, G. (1979) *J. Biol. Chem. 254*, 2968−2974.
44. Wawrzynow, A., Collins, J. H., and Coan, C. (1993) *Biochemistry 32*, 10803−10811.
45. Coan, C., and Keating, S. (1982) *Biochemistry 21*, 3214−3220.
46. Chen, Z., Coan, C., Fielding, L., and Cassafer, G. (1991) *J. Biol. Chem. 266*, 12386−12394.
47. Coan, C., Ji, J. Y., and Amaral, J. A. (1994) *Biochemistry 33*, 3722−3731.
48. Lewis, S. M., and Thomas, D. D. (1992) *Biochemistry 31*, 7381−7389.
49. McCray, J. A., and Trentham, D. R. (1989) *Annu. Rev. Biophys. Biophys. Chem. 18*, 239−270.
50. Dean, W. L., and Tanford, C. (1978) *Biochemistry 17*, 1683−1690.
51. Kosk-Kosicka, D., Kurzmack, M., and Inesi, G. (1983) *Biochemistry 22*, 2559−2567.
52. Andersen, J. P., Larson, K., and Møller, J. V. (1985) *J. Biol. Chem. 260*, 371−380.

53. Kanazawa, T., Yamada, A., Yamamoto, T., and Tonomura, Y. (1971) *J. Biochem.* (*Tokyo*) *70*, 95−123.
54. Shigekawa, M., Dougherty, J. P., and Katz, A. M. (1978) *J. Biol. Chem. 253*, 1442−1450.
55. Sumida, M., Wang, T., Schwartz, A., Younkin, C., and Froehlich, J. P. (1980) *J. Biol. Chem. 255*, 1497−1503.
56. Pickart, C. M., and Jencks, W. P. (1982) *J. Biol. Chem. 257*, 5319−5322.
57. Mahaney, J. E., and Thomas, D. D. (1991) *Biochemistry 30*, 7171−7180.
58. Squier, T. C., and Thomas, D. D. (1989) *Biophys. J. 56*, 735−748.
59. Gornall, A. G., Bardawill, C. J., and David, M. M. (1949) *J. Biol. Chem. 177*, 751−766.
60. Peterson, G. L. (1977) *Anal. Biochem. 83*, 346−356.
61. Froehlich, J. P., Sullivan, J. V., and Berger, R. L. (1976) *Anal. Biochem. 73*, 331−341.
62. Knott, G. D. (1979) *Comput. Programs Biomed. 10*, 271−280.
63. Hobbs, A. S., Albers, R. W., and Froehlich, J. P. (1980) *J. Biol. Chem. 255*, 3395−3402.
64. Inesi, G., Kurzmack, M., Coan, C., and Lewis, D. E. (1980) *J. Biol. Chem. 255*, 3025−3031.
65. Beeler, T., and Keffer, J. (1984) *Biochim. Biophys. Acta 773*, 99−105.
66. Inesi, G., Kurzmack, M., Kosk-Kosicka, D., Lewis, D., Scofano, H., and Guimaraes-Motta, H. (1982) *Z. Naturforsch. C 37*, 685−691.
67. Yu, X., and Inesi, G. (1995) *J. Biol. Chem. 270*, 4361−4367.
68. De Meis, L. (2001) *J. Biol. Chem. 276*, 25078−25087.
69. Compos, M., and Beauge, L. (1997) *Ann. N.Y. Acad. Sci. 834*, 378−380.
70. Jørgensen, P. L., and Pedersen, J. (1985) *Biochim. Biophys. Acta 821*, 319−333.
71. Møller, J. V., Guillaume, L., Marchand, C., Montigny, C., le Maire, M., Toyoshima, C., Staehr Juul, B., and Champeil, P. (2002) *J. Biol. Chem. 277*, 38647−38659.
72. Makinose, M., and Hasselbach, W. (1971) *Fed. Eur. Biochem. Soc. Lett. 12*, 271−272.

BI035068G